2-1-2014

Studying the molecular dynamics of deuterium molecules trapped inside a simple clathrate hydrate using high resolution Raman spectroscopy

Mohamed Ibrahim Moussa Ibrahim

The American University in Cairo

School of Sciences & Engineering

"Studying the Molecular Dynamics of Deuterium Molecules trapped inside a Simple Clathrate Hydrate Using High Resolution Raman Spectroscopy"

A Thesis submitted to

The Physics Graduate Program

In partial fulfillment of the requirements for the degree of

Master of Science

By

Mohamed I. Mousa

Supervisor: Prof. Salah El.Sheikh

Physics Department, The American University in Cairo

Co-Advisors: Dr. Lorenzo Ulivi, Dr. Milva Celli

Institute of Complex Systems, National Research Center, Florence, Italy

September 2013

DEDICATION

"I dedicate this research to the all innocent people that died in Egypt at the last events followed ousting of Mohamed Morsi, especially, my friends Habiba Ahmed Abdel Aziz and Abdel Hameed Sobeah"

ACKNOWLEDGEMENTS

Thanks to Allah for all his support in my life.

Thanks to my parents for your continuous encourage and help to finish this dissertation. Without you, nothing would be done. I promise I will always make you proud of me.

To Dr. Salah El-Sheikh, you have assisted me to join the program, to pursue my experimental work in Italy. Without your guidance and persistence help this dissertation would not have been possible. You are my godfather.

To Dr. Lorenzo Ulivi and Dr. Milva Celli, you have hosted me in your laboratory, allowed me to use your equipment, taught me how to be a good experimentalist, and helped me to analyze the experimental data. It is a pleasure for me to know you and to work with you.

To Moaaz El Ghazaly, you are the best companion. We have experienced every moment in our careers together. Hope that if we can get the PhD together.

To Mohamed Zaghloul, thank you for your information that you have provided. Without you, the stay in Italy would be harder.

Great thanks to my colleagues and friends in physics department. It was a pleasure for me to work, laugh, discuss

with you. You have helped me a lot and I will never forget you.
To my sisters Mona and Maha, thanks a lot for your patience, love, and kindness. Especial thanks to Mona for lending me her laptop.

Thanks to my fiancée, Yasmin, that encouraged me to do this research. You have afforded my hard times. Without your motivation, the thesis will take more time to be finished.

Thanks to Yasmin's family, Nevin, Hisham, uncle Ezzat, aunt Taghred, for your solid support.

Thanks to the all people that help me to get this final form of the thesis.

ABSTRACT

As the energy resources running out, scientists are trying to provide sustainable energy. They move toward the hydrogen economy although it has large technical difficulties that need to be solved. Hydrogen is considered as a clean fuel. Storing hydrogen using clathrate hydrates is one of the promising ways to provide required energy. The high hydrogen content in sII clathrate hydrate proposes some applications like replacing gasoline to fuel vehicles, using as a gas separation substance, and transporting some dangerous gases.

In addition, clathrate hydrate is found in nature in huge amounts. Generally speaking, it is approximated that about 3000 billion tons of carbons of clathrate hydrates exist as a worldwide reserves. This large amount can replace usual fossil fuel like oil and coal, and be a new energy source. All what we need is to investigate these compounds and find the ways to make use of them.

Clathrate hydrates are inclusion compounds, physically resembles ice, can trap a guest small non polar molecule behind walls made by water via confining the guest molecules by a definite structure. So, it isn't a chemical storage but physical. From the historical point of view, it is thought that the hydrogen and its isotopes are very small to make clathrate compounds stable but, recently, it is used to build a simple cubic structure II with water molecules. Formation of clathrate hydrates depends on the applied high pressure, low temperature, and the guest molecule.

In this research, a full detailed picture of deuterium clathrate hydtare including structure, occupancy number per cage, deuterium dynamics, and ortho-para conversion of deuterium inside the cages has been conducted. The storage of deuterium in clathrate hydrate has been tested, and basal concepts of enclathrated deuterium have been evaluated. Manifold cavity occupation and small inter-molecular separation are some new exciting aspects. The small

cages of sII structure can contain one deuterium molecule which represents deuterium content of 1.0 wt%.

Raman spectroscopy is an important tool to study the dynamics of the trapped deuterium and the occupancy of deuterium inside the cages of the clathrate hydrate. It shows the vibrational and rotational bands of deuterium molecules. In sII hydrates, we have two types of cages: small cages and large cages. Enclathrated deuterium at all cages vibrates at lower frequency than free gas phase. In addition, the single deuterium occupied cages vibrates at lower frequency than multiple deuterium occupied cages.

Raman spectra was collected from many samples of in-situ prepared deuterium clathrate placed in a cell to see the formation of the clathrate structure and the changes occur while applying heating and quenching cycles. Analysis of the vibrational bands of different cages has been explored and calculations regarding average occupancy number have been done.

TABLE OF CONTENTS

LIST OF FIGURES

Chapter 1 INTRODUCTION TO CLATHRATE COMPOUNDS, CLATHRATE HYDRATES AND HYDROGEN CLATHRATES

1.1 Clathrate Compounds

Clathrate compounds are inclusion compounds of host molecules; make a network of bonds of different sizes and shapes, and a guest molecule. There is no any chemical bond between the guest molecules and host molecules. These compounds are formed under particular low temperature and high pressure in addition to the presence of the guest molecule. Without the guest molecules, the structure of the clathrate will collapse and will be a normal ice crystal structure. There are some similar properties between clathrate hydrates and conventional ice but clathrates are stable above 273.15 K. [1]

Historically, the name **clathrate** is derived from the Latin **clathratus** that means enclosed by bars or network. Powell did this in 1948. In 1778, Joseph Priestley may have been the first to discover clathrates taking advantage of the cold winters in Birmingham to refrigerate his samples of sulfur dioxide and water. Credit for the discovery is usually given to Michael Faraday's boss, Sir Humphry Davy who reported a clathrate in the chlorine and water system in 1811. [2]

1.2 Clathrate Hydrates

To be more specific, we will focus on a special type of clathrate hydrates made from trapped deuterium gas and water cages (~ 1nm in size). They both form what we call deuterium hydrate. It needs to be investigated because it is considered an energy resource and a clean fuel. This research is a cutting-edge level and fits with the local and international needs of energy resources. To study deuterium clathrate, we can use many spectroscopic techniques like IR, near UV and neutron diffraction but our concerning here is to study it using Raman spectroscopy. Raman spectroscopy is one of the most powerful techniques to study both vibrational and rotational modes of the system. It depends on the inelastic scattering of a monochromatic line (a laser beam) by the guest molecule. The laser beam will interact with the vibrational bands, phonons of the guest molecule, rotational bands, or any other excitations in the system to give us a full detailed picture about the guest molecule.

Clathrate hydrate formation conditions differ according to the volume of the guest molecules. Clathrate hydrates have three crystal structures like cubic sI, sII and hexagonal sH. These structures have space groups of *Pm3n, Fd*$\bar{3}$*m* and *P6/mmm* respectively. The radii of the cages depend on the volume of the guest molecule. The cage's form is a polyhedron of pentagonal faces or hexagons. The most common three structures are shown in figure 1.5.

To determine the geometry of the cage we can use the following nomenclature:

$$A^x B^y$$

Where A and B is the shape of the face (pentagon or hexagon), and x and y are the number of sided faces in the cavity. For example, 5^{12} mean that we have twelve pentagonal faces to form the cage. Figure 1.1 show the geometry of possible clathrate hydrates cavities.

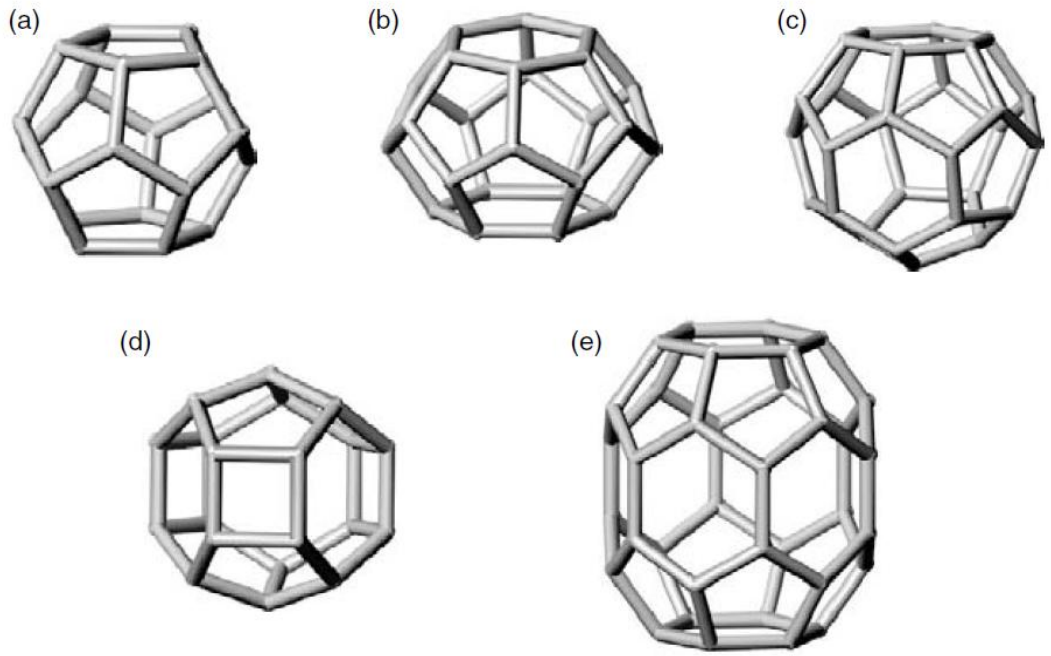

Figure 1.1. The geometry of possible clathrate hydrates cavities: (a) pentagonal dodecahedron (5^{12}), (b) tetrakaidecahedron (5^{12} 6^{2}), (c) hexakaide-cahedron (4^{3} 5^{6} 6^{3}), and (e) icosahedron (5^{12} 6^{8}). [1]

The first unit cell of type sI (*Pm3n* space group) contains 46 water molecules, generating two types of cages: small and large. A pentagonal dedecahedron (5^{12}) will be the shape of the small cage but the large cage will have a tetradecahedron (5^{12} 6^2) (figure 1.2).

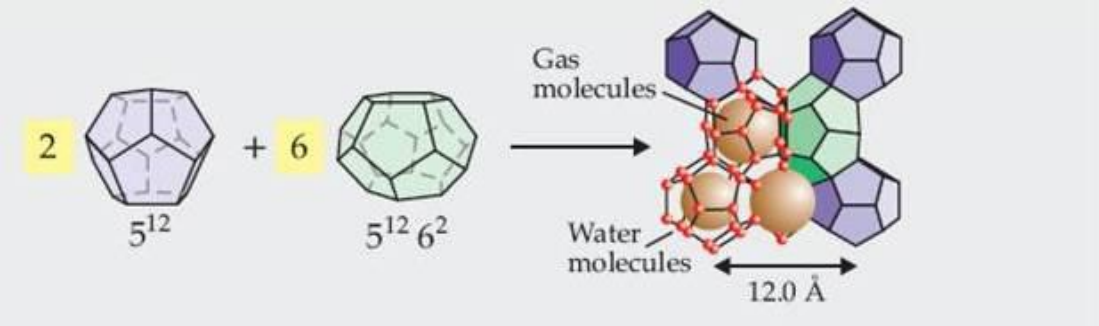

Figure 1.2. Two small cages (5^{12}) in addition to six large cages (5^{12} 6^2) makes the unit cell of sI crystalline structure with an average lattice constant (a ~ 12 Å). [3]

The second unit cell of type sII (*Fd*$\bar{3}$*m* space group) contains 136 water molecules, generating two types of cages: small (average radius 3.95 Å) (5^{12}) and large (average radius 4.33 Å) (5^{12} 6^4). The case of sII like the case of sI but the shape of the large cage is a hexadecahedron (figure 1.3).

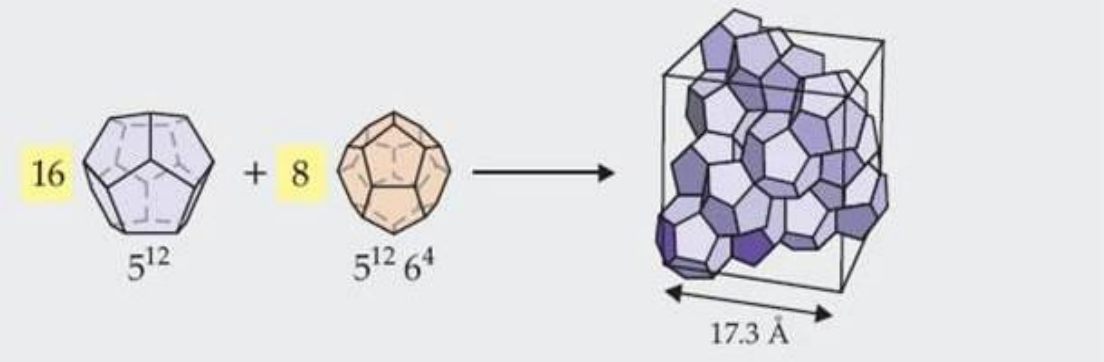

Figure 1.3. Sixteen small cages (5^{12}) in addition to eight large cages (5^{12} 6^4) makes the unit cell of sII crystalline structure with an average lattice constant (a ~ 17.3 Å). [3]

The third unit cell of type sH (*P6/mmm* space group) contains 34 water molecules producing three cages. The three cages are two small cages different in type and one large. To form type H, the two guest molecules (large one and

small one in size) must cooperate to make the compound stable. The large guest molecule will fit in the large cage giving the help to fill other smaller cages (figure 1.4).

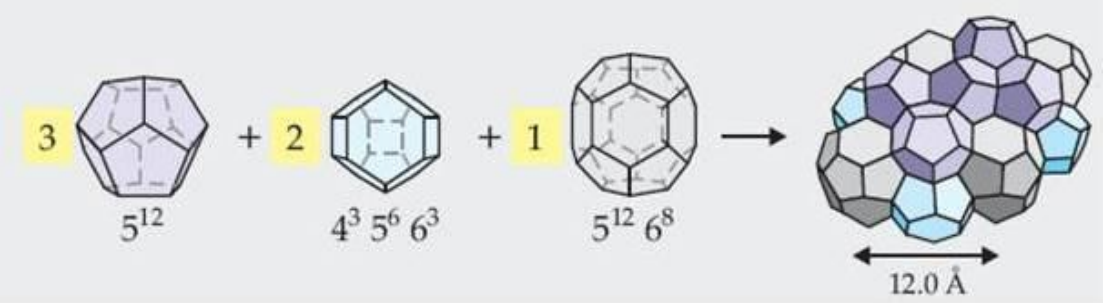

Figure 1.4. Three small cages (5^{12}) in addition to two mid cages ($4^3\,5^6\,6^3$) and one large cage ($5^{12}\,6^8$) makes the unit cell of sH crystalline structure with an average lattice constant (a ~ 12 Å). [3]

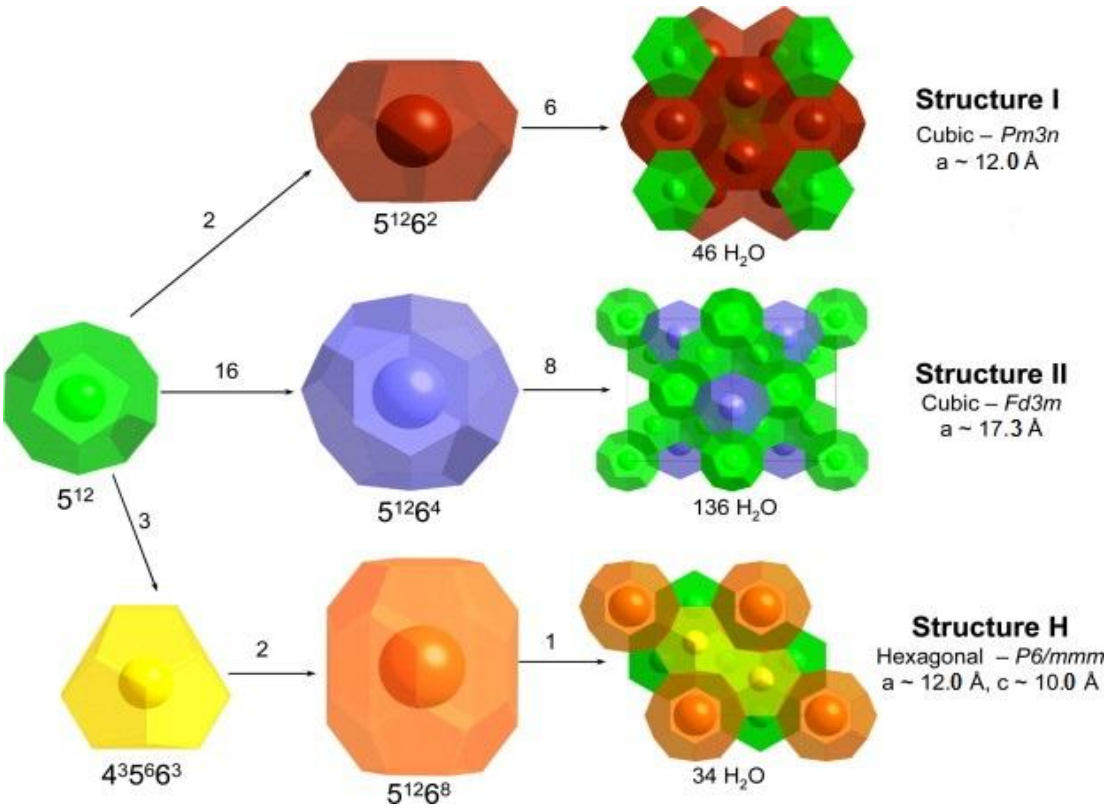

Figure 1.5. The possible three common clathrate hydrate structures. [2]

Although the chemistry of the trapped molecule affects the structure shape and stability of the compound strongly, [4] the structure formation depends on the size of the guest molecule.

Gases ranging in size (d ~ 4-6 Å) like carbon dioxide CO_2, methane CH_4, ethane C_2H_6 and hydrogen sulfide form sI structure of *Pm3n* space group with a unit cell consists of two small (5^{12}) cages and six large (5^{12} 6^2) cages with an average lattice constant (a ~ 12 Å).

Molecules ranging in size (d ~ 4 Å) like nitrogen N_2, or less than (d < 4 Å) like hydrogen H_2 in addition to bigger molecules ranging in size (d ~ 6-7 Å) like propane C_3H_8, can form sII structure of $Fd\bar{3}m$ space group with a unit cell consists of sixteen small (5^{12}) and eight large (5^{12} 6^4) cavities with an average lattice spacing (a ~ 17.3 Å).

To form sH structure, two different species are needed to make the clathrate stable. One large organic guest molecule (d ~ 7.5 - 9 Å) like methylcyclohexane, iso-pentane, or 2,2-dimethylbutane should occupy the large (5^{12} 6^8) cavity which is one per unit cell. Another small guest molecule like deuterium D_2, hydrogen H_2 and methane CH_4 should be stored inside (4^3 5^6 6^3) cavity (two per unit cell) beside (5^{12}) cavity (three per unit cell). Therefore, we have in this case two lattice constants (a ~ 12, c ~ 10 Å) and the space group is *P6/mmm*. Figure 1.6 show dependence of the formed structure on the size of the guest molecule.

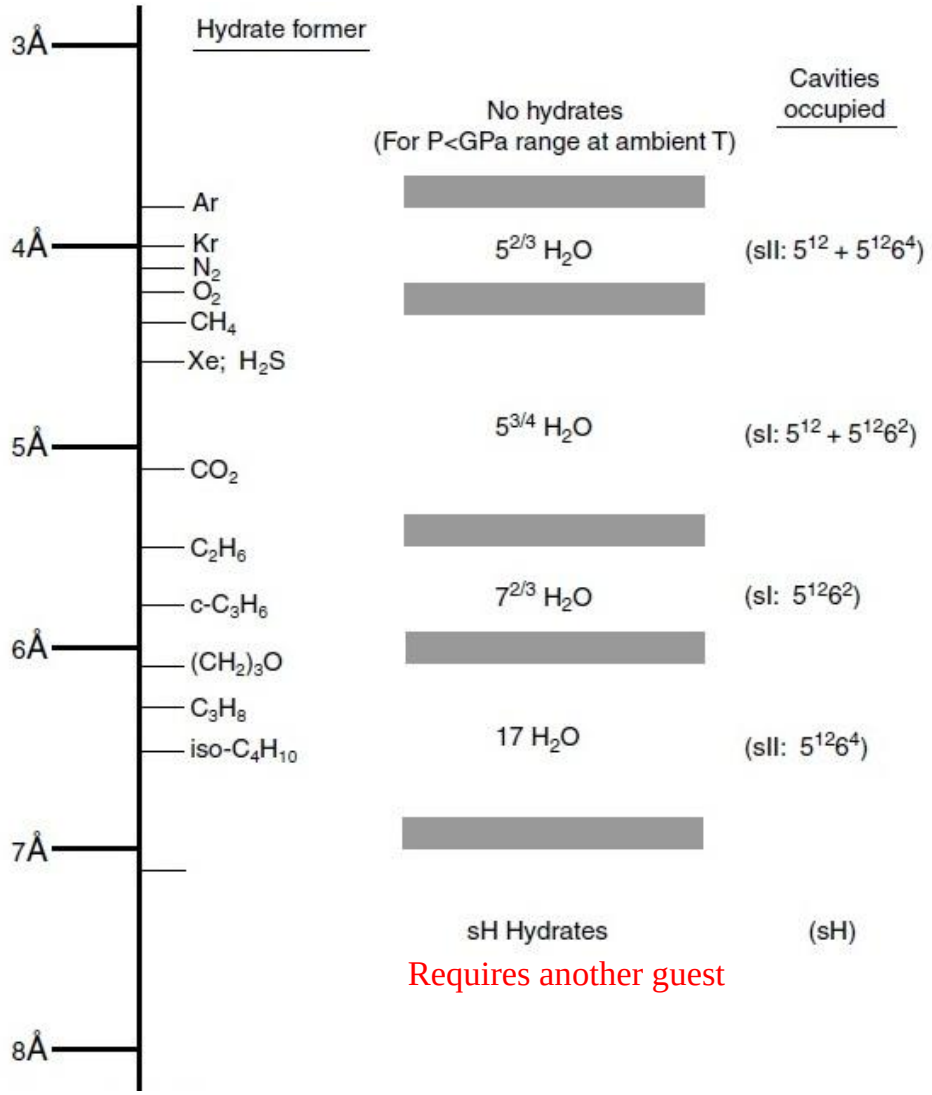

Figure 1.6. Comparison of guest molecule sizes and cavities occupied as simple hydrates. [5]

1.3 Hydrogen Clathrates

If the former of the clathrate hydrate is the hydrogen gas, it is called hydrogen clathrate hydrate. Monatomic hydrogen is the smallest abundant element on the earth. [6] Due to its small size, it was thought that it could not provide stability for clathrate hydrate phase. [7] However, in the last decade, it is proven experimentally that hydrogen can make stable clathrate compounds regardless of being alone (simple hydrogen hydrate) or enclosed with another guest molecule (binary hydrogen hydrate) like tetrahydrofuran (THF). [8] Dihydrogen (H_2) is a hydrophobic (hate water), highly combustible, nonmetallic element in addition to being a clean fuel. Storing hydrogen in tanks using liquefying ways is a very jeopardizing task due to the high combustion of the hydrogen. In addition, it is very expensive process. Therefore, scientists moved to investigate new efficient economic safe mean of storage. Hydrogen hydrates is a promising material to do so. It offers appreciable solutions for transport and storage of hydrogen.

Hydrogen forms sII clathrate hydrates. This clathrate as mentioned before has a simple cubic unit cell containing 136 water molecules forming sixteen small cages (5^{12}) and eight large cages ($5^{12}\ 6^4$). It is believed that the small cage can hold one hydrogen molecule only, regardless of the type of the clathrate hydrate whether it is simple or binary, while the large cage can afford up to four molecules of hydrogen in case of simple hydrates, or, one large organic compound (such as THF) in case of binary hydrates. [9]

Also, hydrogen can form sI and sH structures but under particular circumstances. It needs another guest molecule with a suitable size to make the clathrate stable. [10]

From the history point of view, Dyadin et al. made the first experiment to study simple hydrogen hydrate ($H_2 + H_2O$) in 1999. [11], [12] The structure of the

clathrate was guessed by comparing the P-T diagram of the hydrogen hydrate sample with known rare gases hydrates (Xe, Kr, Ar) (Figure 1.7).

Mao et al. (2002) [13] did another experiment to give more account about simple hydrogen hydrate. Mao et al. applied high pressure to about 300 MPa using diamond anvil cell on the sample. After cooling the cell to 250 K, a new phase started to raise between the distinct hydrogen and liquid water phases. Mao et al. used Raman spectroscopy and the figure 1.8 is the output of the run. Figure 1.8 shows Raman spectra for hydrogen gas and hydrogen hydrate over a range of temperature and pressure circumstances in the region of H_2 region.

The figure 1.8 illustrates the vibrational bands of trapped H_2 molecules inside the clathrate cages. Beside, these bands have lower frequency than free H_2 molecules, which fits with guest molecules being trapped in the hydrate cages. [14] Additionally, the dissemination and positions of the new peaks introduce the fact that there are small (5^{12}) and large ($5^{12}\ 6^4$) cages (sII structure). Mao et al. reported that the peaks at low frequencies appeared by H_2 inside large cages ($5^{12}\ 6^4$), while the peaks at high frequencies resulted from H_2 in small cages (5^{12}). This assumption was based on the fact that some clathrates are stable with single large cavity occupancy in addition to the intensity decrease of the high frequencies peaks with temperature.

Mao et al. compared the areas of peaks of hydrogen in both hydrate and gas phase in addition to volumetric ratio of the two phases inside the cell to calculate hydrogen to water ratio. The ratio was about 0.45 and represented hydrogen content of ~ 5.3 wt%. Based on this H_2:H_2O ratio, Mao and his colleagues tried to guess the possible structure that fits with this ratio. Finally, they agreed that two hydrogen molecules occupy the small cages while four hydrogen molecules occupy the large cages.

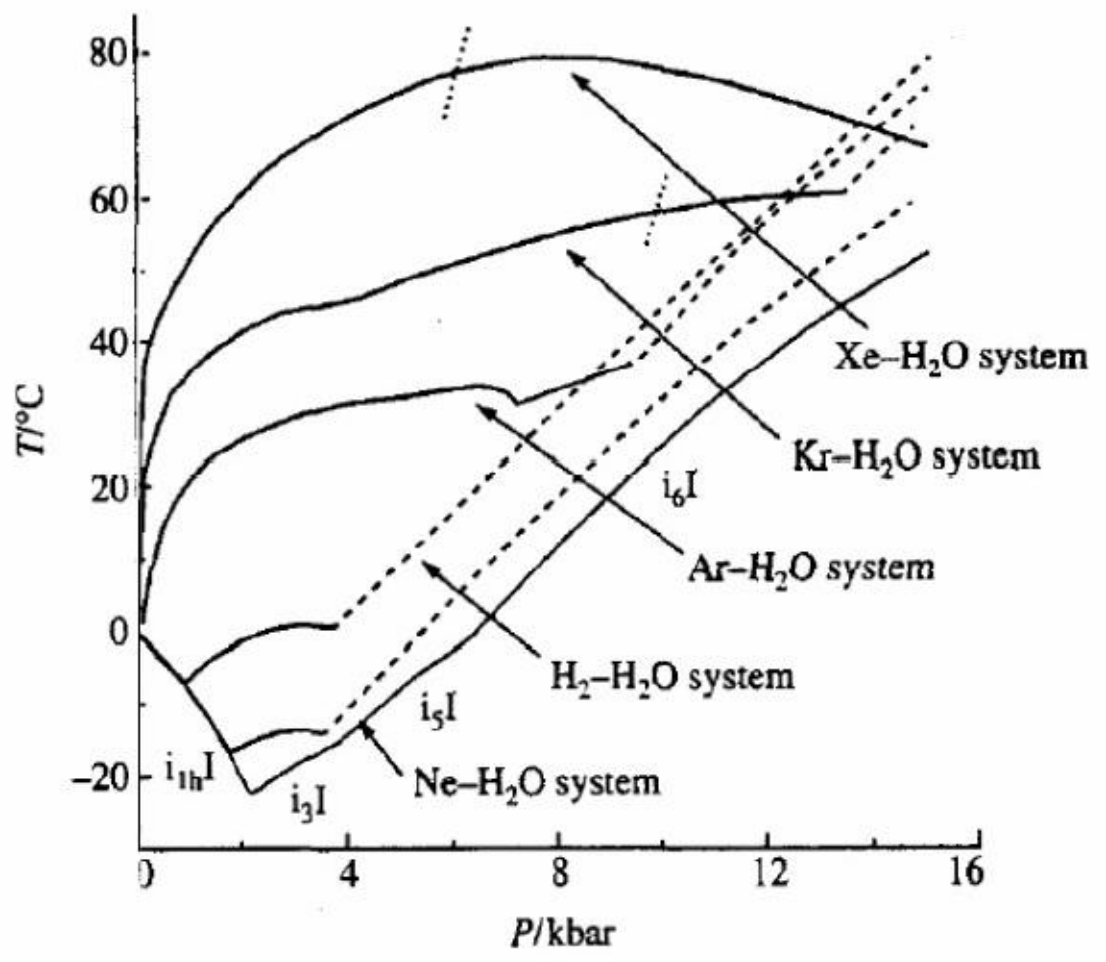

Figure 1.7. P-T diagram for simple hydrogen hydrate compared with other known hydrates of rare gases. [11]

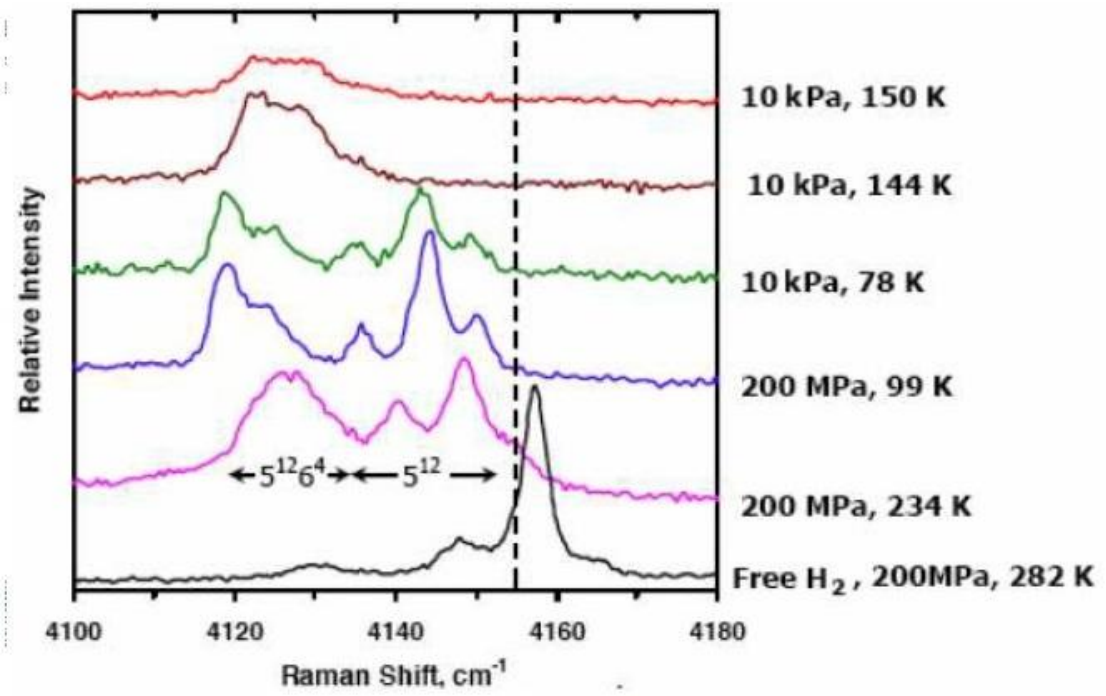

Figure 1.8. Raman spectra of hydrogen hydrate in H_2 vibration region. [13]

On the contrary to what Mao et al. did, Lokshin et al. [15] reported one hydrogen (D_2) molecule occupied the small cages while the large cavities contains two to four molecules depending on the applied pressure and temperature in 2004. The structure still sII. Figure 1.9 shows the occupancy of small and large cages at 2000 bar and 1 bar as a function of temperature.

Moreover, Lokshin et al. found that the distance D_2-D_2 is 2.93 Å when the large cavity is filled with four hydrogen molecules. The arrangement is tetrahedral. This distance is very distinctive because the intermolecular distance between solid hydrogen molecules is 3.78 Å at 1 bar and 4.2 K. [16] As a result of this characteristic distance, the potential of hydrogen hydrates storage has increased as the energy density may be abnormally high. Figure 1.10 shows the arrangements of D_2 molecules.

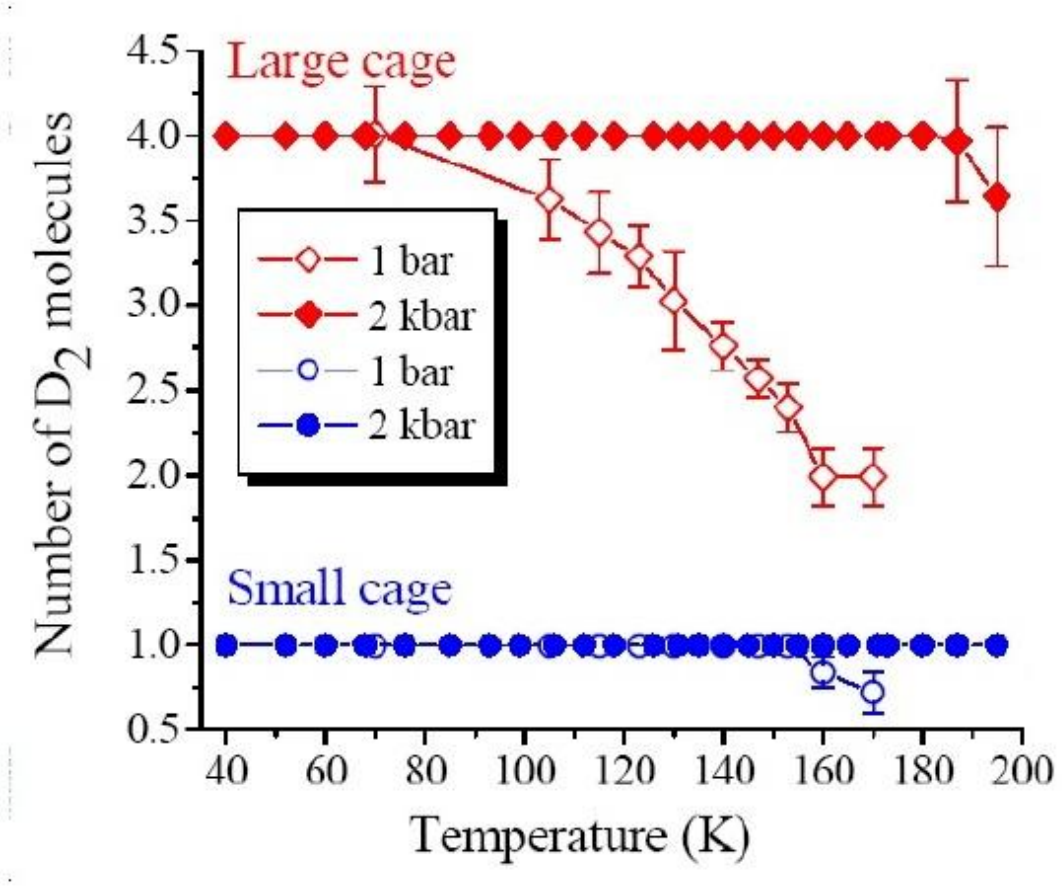

Figure 1.9. The occupancy of small and large cages at 2000 bar and 1 bar as a function of temperature. [15]

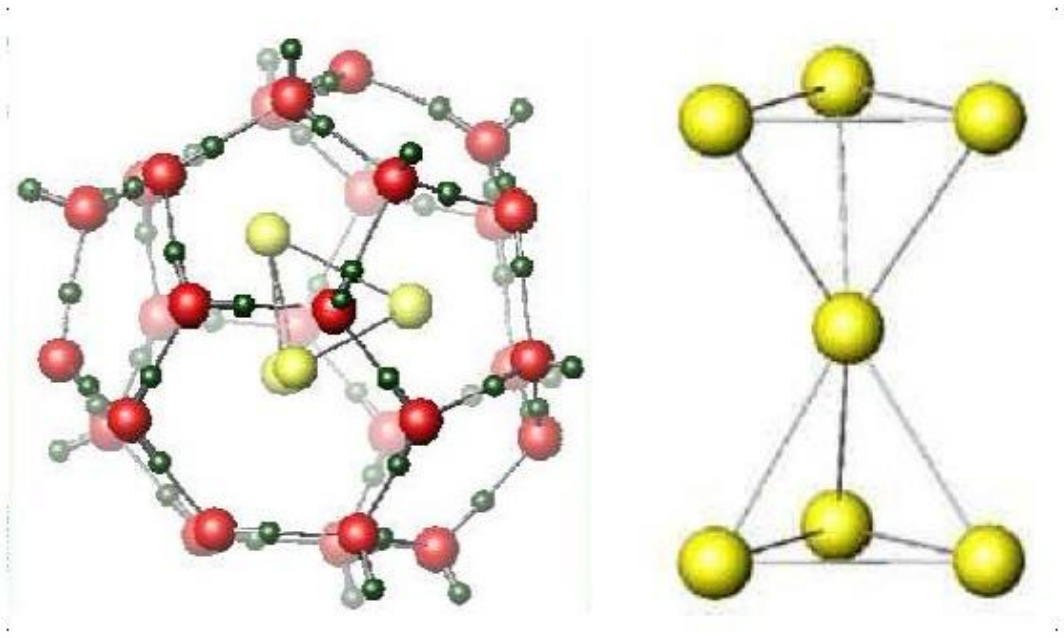

Figure 1.10. Arrangments of hydrogen molecules: (left) D_2-D_2 distance of 2.93 Å in the large cavity at 50 K and 1 bar, (right) H_2-H_2 distance of 3.78 Å in solid hydrogen at 4.2 K and 1 bar. [15]

1.3.1 Hydrogen Hydrates as Future Fuel

Scientists and engineers always seek for solutions to the problems that face the world, especially those related to energy. It is expected that the usual fossil fuel sources like petroleum and coal will be finished within the upcoming years. We need to find new energy sources. Clathrate hydrates can provide the world with sufficient amount of energy. Around 6.4 trillion tons of mathane hydrates be present on ocean floor. [17]

The world moves toward hydrogen economy because it is considered clean and environmentally friend. In recent years, some research have been done to investigate hydrogen hydrate properities. they revealed unique properities of clathrates that made the clathrate a hot topic of research. Hydrogen is transported by liquefying the gas under high pressure and low temperature in tanks. This technique is expensive, dangerous, needs particular tools to maintain these conditions. Clathrates can be used to store and transport of hydrogen in efficient economic safe mean. Actually, one of the main challenges to hydrogen economy is to prvide high energy density similar to available liquid transportation fuels. [18]

Simple hydrogen hydrates have many advantages: the trapping material is just water, the formation and dissociation is so quick, [19] no chemical reacion is required to release hydrogen from the clathrate, and water is cheap.

1.4 Hydrate Formation and Dissociation Processes

The clathrate hydrate formation and dissociation processes are not well understood until now. At the common pressures, in the three hydrate structures, each cavity can contain at most one guest molecule. At very high pressures, nitrogen, hydrogen, methane, and argon can multiply occupy the large cavity of structure II.

Although we need to provide a guest gas with high pressure and water in a low temperature to form the clathrate, some clathrates are formed at high temperatures above 300 K and at subatmospheric pressures relying on the forming gas. [7]

To make a simple hydrogen hydrate, it is found that the synthesis pressures required to form it around 100 MPa in low temperatures. If we want to form the clathrate at higher temperatures like 273 K, we should increase the applied pressure as well to 200 MPa. Therefore, we can control the formation process through two options: lowering the temperature, or, raising the pressure. Both have the same effect but the formation process needs more time in case of lowering the temperature because molecules become less energetic. Figure 1.11 shows P-T diagram of hydrogen hydrate formation conditions.

The optimum conditions to make sII hydrogen hydrates stable are: pressure ~ 220 MPa, and, temperature at 249 K. This structure is transformed to a filled ice II structure when the pressure increases to 1 GPa. With further increasing of the pressure to 2 GPa, the structure transforms to cubic ice Ic. [20]

To study the formation process, we need to go down to the microscopical scale. The hydrate formation is a stochastic process that means it is non-determministic state, needs a supersaturated system to happen. [21] It is considered one of the crystallization processes.

Crystallization process consists of two stages. The first stage is the nucleation includes the formation of the hydrate nuclei. [21] Nucleation is the

stage that the diffused solute molecules induces a gathering process to form clusters, generating a small solute aggregate in a nanometer region, that become stable under the operating conditions. If this aggregate isn't stable, it will redissolve again in the liquid. As a result, the clusters need to reach the critical volume in order to be stable and prevent redissolving. The critical volume is controlled by the driving force of the phases. This driving force results from the difference in the chemical potential between the initial phase and the new phase. [22] Its amount depends on the temperature, pressure, concentration difference and the operating conditions. [23]

The second stage of hydrate formation process is the hydrate growth. The hydrate growth begins following formation of a stable hydrate nuclei. The growth continues until the exhaustion of the supersaturation. At this moment, the crystallization process is complete and an equilibrium occurs among different interfaces.

There are two techniques for the formation of hydrogen hydrate. The first technique: we can allow pressurized hydrogen gas to diffuse into powdered ice whether their structure is ice-II or ice-Ih. [19] In this technique, the interface is gas-solid and it is called solid-state phase transition. The second technique: we allow pressurized hydrogen to diffuse into water, making a liquid solution of hydrogen in water, then starts to cool down the sample, so the clathrate starts to be formed. [24] In the second technique, there are two cases: low and high pressure. In case of low pressure (i.e. low concentration of hydrgen solution), the clathrate is generated at the gas-liquid interface . In case of high pressure, it is thought that there are some particular cages in the supecooled water to host hydrogen solution inside. [25]

To collapse the hydrogen hydrate, we need to increase the temperature to the ambient temperature, or, leaving the compound at 150 K and 1 bar for a long time, as they start to lose the hydrogen gas trapped inside.

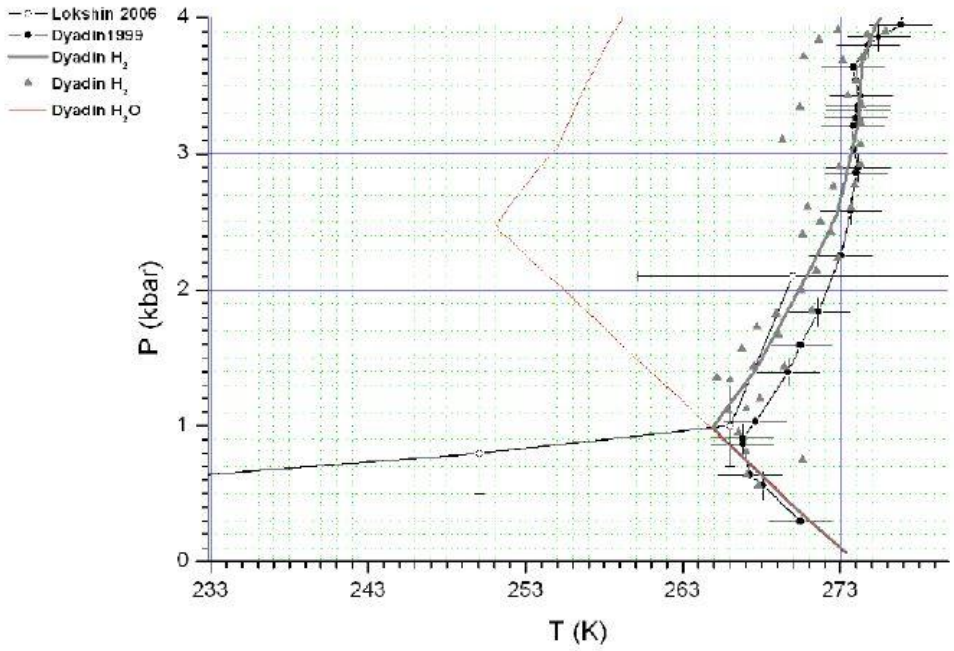

Figure 1.11. P-T diagram of the formation conditions of hydrogen hydrates done by Dyadin, [11][12] Lokshin, [15] and Duarte. [26]

1.5 Thesis Objectives and Outline

The aim of this research is to study the molecular dynamics of trapped deterium (D_2) molecules in sII simple hydrates using high resolution Raman spectroscopy in addition to some important aspects like multiple cage occupation and small inter-nuclear distance of D_2 as they control the hydrogen storage inside hydrates. In addition, there will be an account of ortho-para conversion in case of free gas and inside the cages of the clathrate. Furthemore, it is an opportunity to study the quantum dynamics of confined hydrogen in a well defined external potential. Previous work in various literatures has been introduced, followed by addressing of the problem. Solutions and recommendations will be stated to problems mentioned above through comprehensive investigation of the experimental work done in this research.

In Chapter 2, a full detailed picture of the Raman spectroscopy theory from both classical and quantum views shall be presented.

In Chapter 3, studying the behavior of hydrogen hydrates using Raman spectroscopy and challenges regarding the assignment of the vibrational peaks will be introduced.

In Chapter 4, account of the experiment equipment, procedure, results, data analysis and discussion will be presented in full details.

In Chapter 5, different applications of clathrate hydrates in addition to some recommendations for future work.

Chapter 2 THE THEORY OF RAMAN SPECTROSCOPY

2.1 Raman Spectroscopy

Raman spectroscopy is one of the most important spectroscopic techniques that are used to study the molecular dynamics of molecules and atoms. It gives details regarding vibrational and rotational bands of them. It depends on inelastic scattering of a monochromatic beam, a laser beam at the visible range. The laser beam interacts with the vibration and rotation of the molecule. The molecules absorb the incident photons energy of the laser beam, they become excited and move up to virtual states. At this moment, there are three cases for the excited molecules:

1- To go back to the original energy level emitting a photon with energy equal to the incident photon energy without any loss. This is called Rayleigh scattering (see figure 2.1).

2- To go back to a higher vibrational level emitting a photon with an energy lower than the incident photon energy making a loss of amount $\Delta\nu$. This is called Stokes Raman scattering (see figure 2.2).

3- To go back to lower vibrational level emitting a photon with an energy higher than the incident photon energy making a gain of amount $\Delta\nu$. This is called anti-Stokes Raman scattering (see figure 2.3).

Therefore, the rotational and vibrational frequencies of the scattered molecule by the incident light appear as difference frequencies with respect to the Rayleigh scattering. Figure 2.4 shows a complete Raman spectrum for a diatomic molecule.

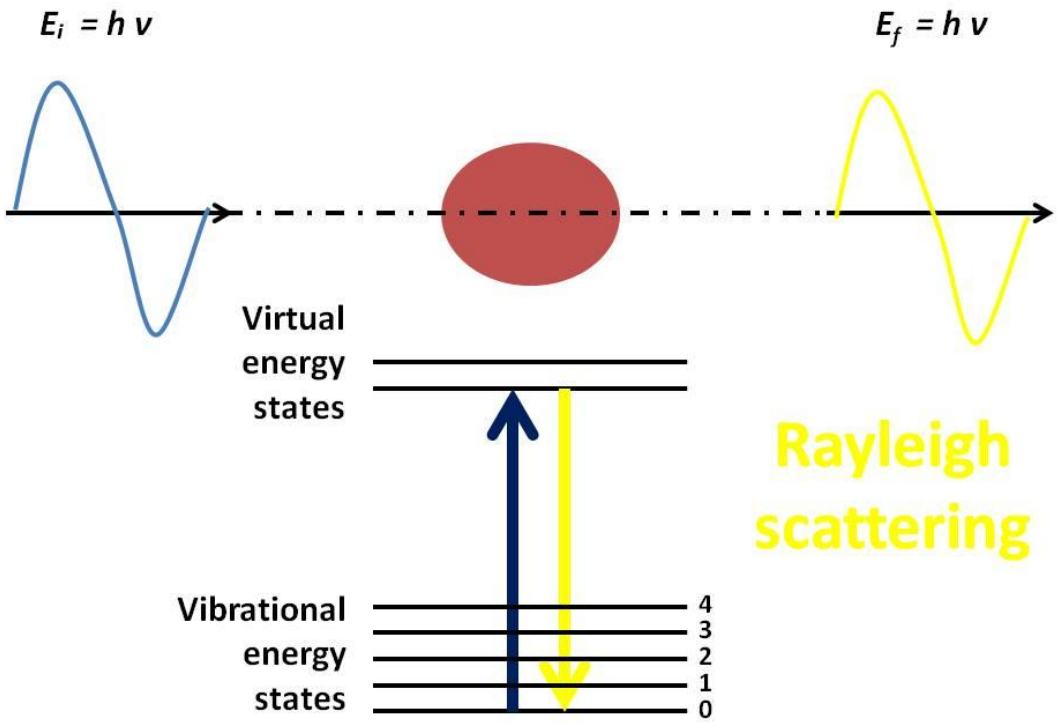

Figure 2.1. Shows the Rayleigh scattering process and there is no loss in energy between the incident and scattered photon.

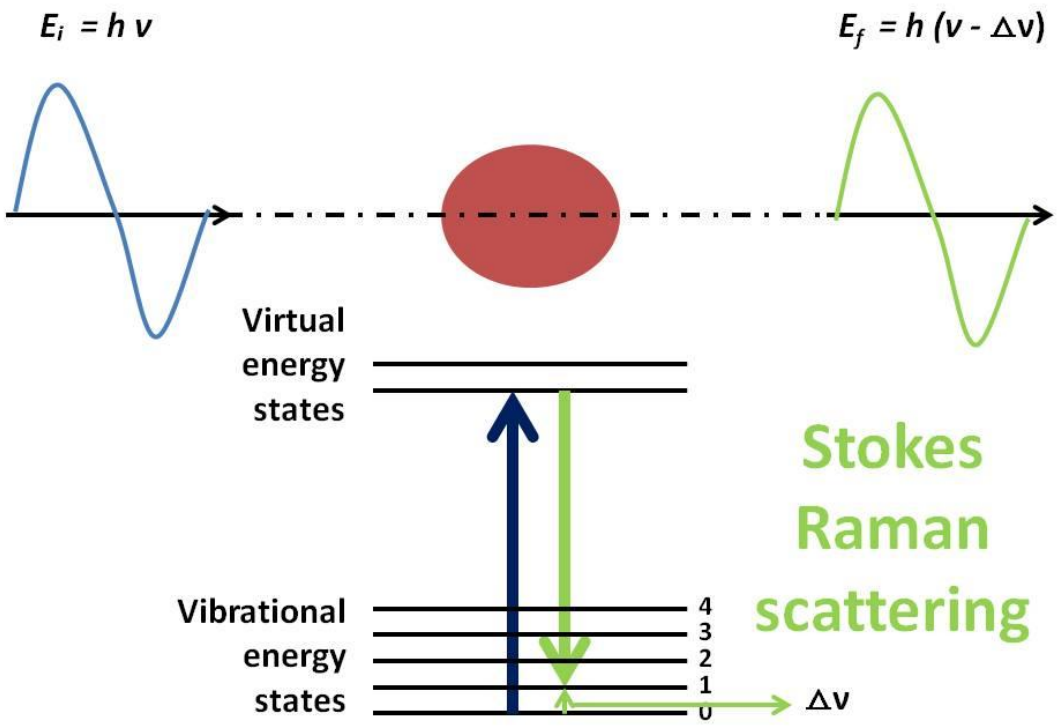

Figure 2.2. Shows the Stokes Raman scattering and there is a loss in energy with amount $\Delta\nu$ between the emitted and incident photon.

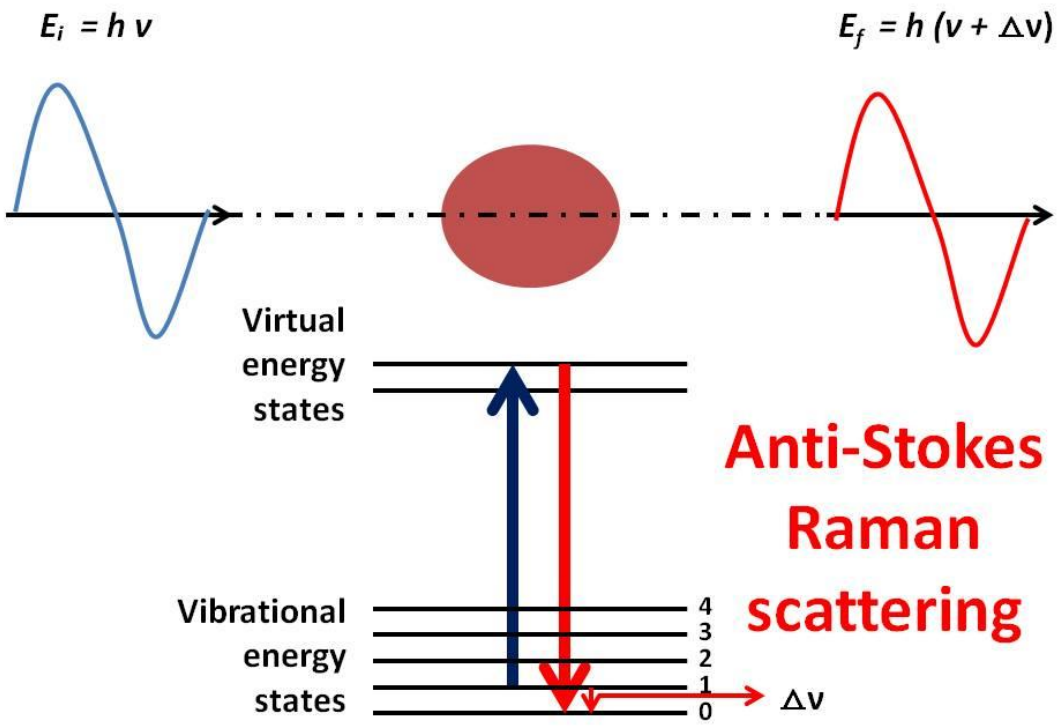

Figure 2.3. Shows the anti-Stokes Raman scattering and there is an increment of amount $\Delta\nu$ between the emitted and incident photon.

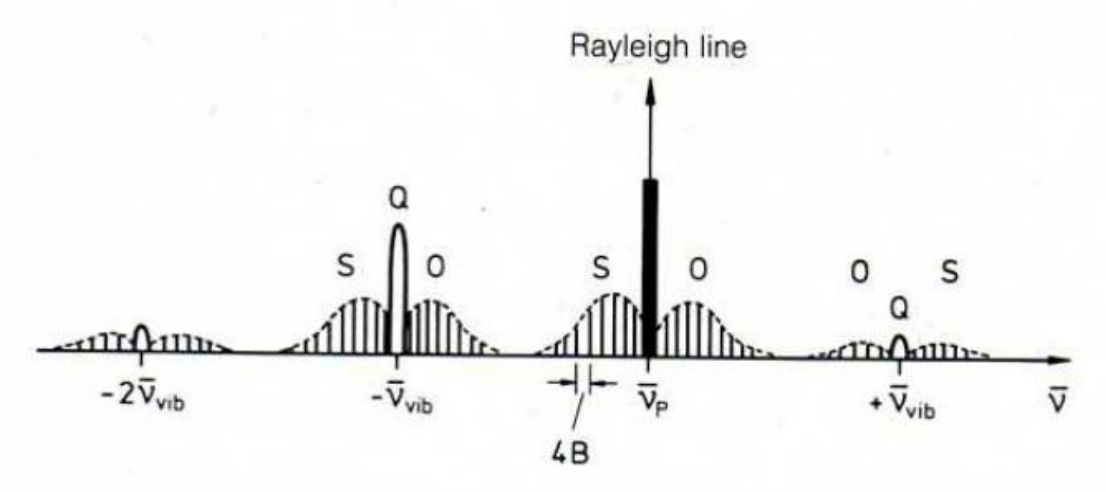

Figure 2.4. The figure shows a complete Raman spectrum of a diatomic molecule. The Rayleigh line at a frequency $\overline{\boldsymbol{\nu_p}}$ is surrounded by spaced shifted rotational lines. Q, S, and O are the rotational-vibrational Raman lines. From the graph, we can notice that the intensity of the Rayleigh line is the maximum followed by Stokes lines at frequency $(-\overline{\boldsymbol{\nu_{vib}}})$ while anti-Stokes lines (on the right) and the second harmonics are so weak. [27]

2.2 Classical Theory of Raman Scattering

To interpret Raman scattering, there are two ways: classical wave explanation or quantum particle explanation. In the classical wave explanation, we assume that there are two atoms with masses m_1 and m_2 connected together by a bond (with a bond strength K), which is a massless spring in the classical view, and both masses are moving in the outward direction making displacements x_1 and x_2 as shown in figure 2.5.

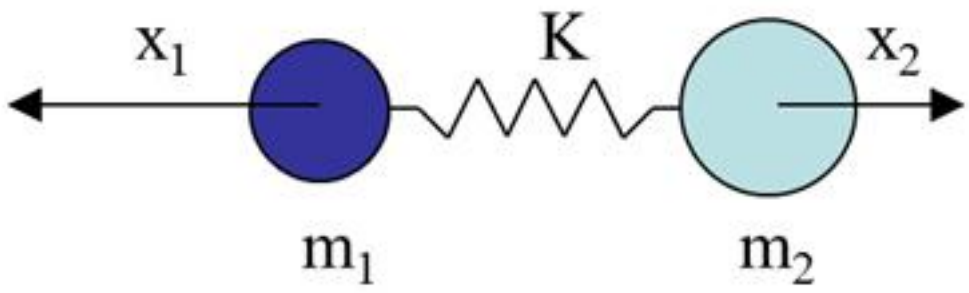

Figure 2.5. Diatomic molecule connected by a massless spring. [27]

By applying the Hooke's law, the equation of motion for this molecule between the atoms can be expressed as following:

$$\frac{m_1 m_2}{m_1 + m_2}\left(\frac{d^2x_1}{dt^2} + \frac{d^2x_2}{dt^2}\right) = -K\,(x_1 + x_2) \quad \text{..... (2.1)}$$

By replacing $m_1 m_2/(m_1 + m_2)$ with μ (reduced mass) and $x_1 + x_2$ with q, the equation can be simplified to,

$$\mu\frac{d^2q}{dt^2} = -Kq \quad \text{..... (2.2)}$$

This equation is simple harmonic equation that can be solved for q we get,

$$q = q_o \cos(2\pi\nu_{vib}t) \quad \text{..... (2.3)}$$

Where ν_{vib} is the molecular vibration frequency and is equal to,

$$\nu_{vib} = \frac{1}{2\pi}\sqrt{\frac{K}{\mu}} \quad \text{..... (2.4)}$$

From equations (2.3) and (2.4), it is so clear that the vibrational frequency is directly proportional with the bond strength and inversely proportional with the reduced mass.

The laser beam is considered an electromagnetic wave associated with a fluctuating electric field E. This electric field reacts with the polarizability of the molecule. The polarizability α of the molecule depends on the interaction of the molecule's electron density with the electric field of the incident wave. Therefore, the incident wave induces a dipole moment P and this dipole moment directly proportional to the electric field by

$$P = \alpha E \quad \text{..... (2.5)}$$

This induced dipole moment vibrates with a definite frequency, hence, the polarization changes with this oscillation. Therefore, the emitted beam will depend on the frequency of polarizability and the frequency of the incident beam. [25] For a light wave with a frequency ν_o, the time varying electric field is given by

$$E = E_o \cos(2\pi\nu_o t) \quad \text{..... (2.6)}$$

Where E_o is the amplitude of the vibrating electric field. From (2.5) and (2.6), so the induced dipole moment can be expressed,

$$P = \alpha E_o \cos(2\pi\nu_o t) \quad \text{..... (2.7)}$$

Such an oscillating dipole emits radiation of its own oscillations with a frequency ν_o, making the Rayleigh scattered beam. If the polarizability changes a little bit than the molecular vibration, so we can use the small amplitude approximation and the polarizability can be a linear function of displacement,

$$\alpha = \alpha_o + q\left(\frac{\partial\alpha}{\partial t}\right)_{q=0} + \cdots \quad \text{..... (2.8)}$$

By substituting (2.3) into (2.8), we can get,

$$\alpha = \alpha_o + q_o \cos(2\pi\nu_{vib}t)\left(\frac{\partial\alpha}{\partial t}\right)_{q=0} \text{……..…... (2.9)}$$

By substitution (2.9) into (2.7), we get,

$$P = \left[\alpha_o + q_o \cos(2\pi\nu_{vib}t)\left(\frac{\partial\alpha}{\partial t}\right)_{q=0}\right][E_o \cos(2\pi\nu_o t)] \text{ ……..... (2.10)}$$

$$P = \alpha_o E_o \cos(2\pi\nu_o t) + q_o \cos(2\pi\nu_{vib}t)\, E_o \cos(2\pi\nu_o t)\left(\frac{\partial\alpha}{\partial t}\right)_{q=0} \text{….. (2.11)}$$

From the last equation, the first part is the Rayleigh scattering component that is the dominant part. The second part is the Raman scattering component.

Using the trigonometric relation

$$\cos\theta\cos\varphi = \frac{1}{2}[\cos(\theta-\varphi)+\cos(\theta+\varphi)] \text{…… (2.12)}$$

Therefore,

$$P = \alpha_o E_o \cos(2\pi\nu_o t) + \frac{1}{2} q_o E_o \left(\frac{\partial\alpha}{\partial t}\right)_{q=0} [\cos(2\pi\{\nu_o - \nu_{vib}\}t) + \cos(2\pi\{\nu_o + \nu_{vib}\}t)] \text{……... (2.13)}$$

The equation (2.13) shows how the dipole moment changes with the frequency. It has three frequency components:

i. (ν_o) with an amplitude $\alpha_o E_o$
ii. ($\nu_o - \nu_{vib}$) with an amplitude $\frac{1}{2} q_o E_o \left(\frac{\partial\alpha}{\partial t}\right)_{q=0}$
iii. ($\nu_o + \nu_{vib}$) with an ampitude $\frac{1}{2} q_o E_o \left(\frac{\partial\alpha}{\partial t}\right)_{q=0}$

Therefore, we expect to get three peaks: one for Rayleigh scattering with a frequency ν_o, one on the left for Stokes Raman scattering with a frequency $\nu_o - \nu_{vib}$, and one on the right for anti-Stokes Raman scattering with a frequency $\nu_o + \nu_{vib}$. See figure 2.6.

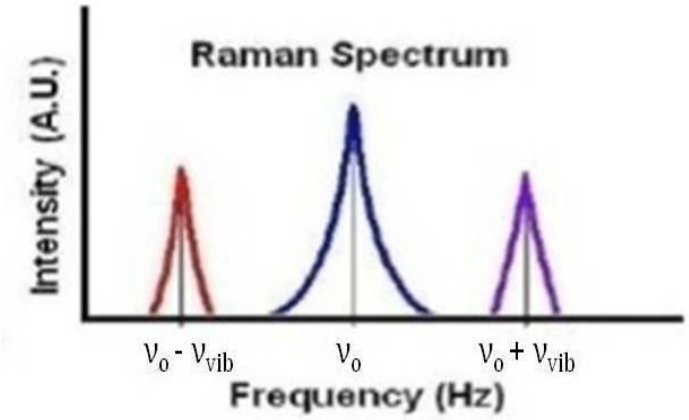

Figure 2.6. The expected three regions, one for Rayleigh scattering at $\boldsymbol{\nu_o}$, one on the left for Stokes Raman scattering at $\boldsymbol{\nu_o - \nu_{vib}}$, and one on the right for anti-Stokes Raman scattering. [28]

The last formulation is applied for both vibrational and rotational motion but, in the rotational motion, we must take into account that the effect of the same electric field that can make the molecule to rotate with the same amount in two different directions. As a result, the equation of the induced dipole moment changes with the rotation frequency like following:

$$P = \alpha_o E_o \cos(2\pi\nu_o t) + \frac{1}{2} q_o E_o \left(\frac{\partial\alpha}{\partial t}\right)_{q=0} [\cos(2\pi\{\nu_o - 2\nu_{rot}\}t) + \cos(2\pi\{\nu_o + 2\nu_{rot}\}t)] \quad (2.14)$$

Where ν_{rot} is the rotational frequency. When the vibration of molecule doesn't change the polarizability of the molecule (i.e $\left(\frac{\partial\alpha}{\partial t}\right)_{q=0} = 0$) so the dipole vibrates only at the incident light's frequency. Therefore, to get Raman scattering in vibrational and rotational motion, there must be a change in the polarizability (i.e $\left(\frac{\partial\alpha}{\partial t}\right)_{q=0} \neq 0$).

In case of homonuclear diatomic molecules like H_2, N_2, or O_2, they do not show any response for IR because there is no permanent dipole moment. On the other hand, they show Raman scattering because the vibration is associated with a change in the polarizability and, hence, change in the dipole moment.

The classical theory succeeded to show the dependence of Raman and Rayleigh on the frequency, and hence, the polarizability but there are serious problems encountered with the classical theory. First, it cannot be applied for the rotational motion. From the rigid rotor model, the rotational frequency ν_{rot} can take any value, so the spectrum must be continuous and this contradicts the experimental results that show discrete lines.

Another limitation of the classical theory, according to equation (2.13), the assumed intensities of both Stokes Raman lines and anti-Stokes Raman lines are the same while this contradicts with the experimental results. To get anti-Stokes Raman lines, we need a population in some higher vibrational energy levels which isn't satisfied in all cases. On the other hand, the Stokes Raman lines arise from the ground energy level, so that it is easy to get them. Therefore, scientists moved to the quantum particle explanation to make the theoretical background fits with the quantitative experimental result.

2.3 Quantum Particle Explanation of Raman Scattering

In the quantum particle explanation, the light is considered a beam of photons with a fixed amount of energy called quanta. The photon energy is directly proportional with the frequency $E = h\nu$. When a photon scatters with a molecule, this molecule absorbs the energy of the incident photon and moves to a higher excited virtual energy state. In this case, the energy state is a combination of rotational and vibrational bands. After a while, the molecule goes back to either the original energy state or a shifted energy state. If the molecule goes back to the initial energy level without any changing in frequency, the collision is an elastic scattering and the spectral line is called Rayleigh line. If the molecule goes back to a higher energy state than the original one, the collision is inelastic collision and the spectral lines called Stokes lines. In case of the molecule goes back to an energy level lower than the original energy state, the process is inelastic and the resulted lines are anti-Stokes lines. [29] Figure 2.7 shows quantum energy transitions for Rayleigh and Raman lines.

Let's assume that the incident photon energy is E_1, and the scattered photon energy is E_2, so the difference in energy is given by

$$\Delta E = E_2 - E_1 \quad \text{..... (2.15)}$$

But $E = h\nu$, So

$$\Delta E = h\nu_2 - h\nu_1 \quad \text{..... (2.16)}$$

In case of Rayleigh scattering,

$$E_2 = E_1 \rightarrow \Delta E = 0 \quad \text{..... (2.17)}$$

In other words,

$$h\nu_2 = h\nu_1 \quad \text{..... (2.18)}$$

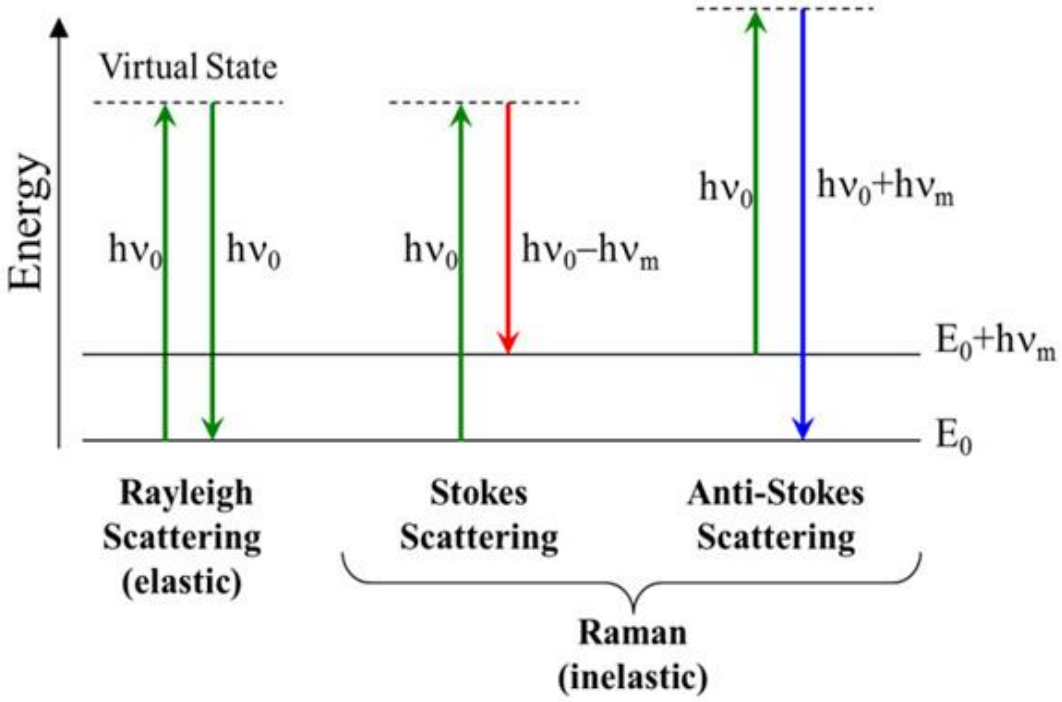

Figure 2.7. Quantum energy transitions for Raman and Rayleigh scattering. [30]

In case of Stokes Raman lines,

$$E_2 < E_1 \rightarrow E_2 = E_1 - \Delta E \quad \text{..... (2.19)}$$

$$h\nu_2 = h\nu_1 - \Delta E \quad \text{..... (2.20)}$$

So, there is a loss of energy with amount (ΔE).

In case of anti-Stokes lines,

$$E_2 > E_1 \rightarrow E_2 = E_1 + \Delta E \quad \text{..... (2.21)}$$

$$h\nu_2 = h\nu_1 + \Delta E \quad \text{..... (2.22)}$$

From the last equation, we found that the molecule has gained energy larger than the incident photon energy.

To study the intensity of Stokes and anti-Stokes lines, we should make a comparison between the populations in the first energy states. We can use Boltzmann distribution. Since, the anti-Stokes lines result from a transition between a higher vibrational-rotational level to a lower one, they needs a population in the original higher level and this opportunity decreases with decreasing the temperature that makes the atoms less energetic and prefer to stay in the ground level than being in a higher energy state.

From Boltzmann distribution function,

$$N_i = Ne^{-\frac{E_i}{k_B T}} \quad \text{..... (2.23)}$$

Where N_i is number of particles occupying the energy state *i*, *N* is the total number of particles, E_i is the energy of the particles, k_B is the Boltzmann constant, and *T* is the temperature of the system, we can study the intensity as following,

$$\frac{I_{anti-Stokes}}{I_{Stokes}} = \frac{n(\nu=1)}{n(\nu=0)} = e^{-\frac{h\nu_{vib}}{k_B T}} \quad \text{..... (2.24)}$$

If we set $\nu_{vib} = 1000\ cm^{-1}$ and $T = 300\ K$, we obtain a numerical value of e^{-5} from the last equation, i.e. 0.7% for the relative intensity. The selection rules in the quantum particle explanation are $\Delta\nu = \pm 1$ (in addition to $\pm 2, \pm 3$, with very low possibilities.

To interpret the rotational transition using the quantum particle treatment, we should first check the geometry of the molecular rotors which can be divided into linear, spherical, symmetric and asymmetric rotors. For H_2, N_2, and O_2, they are considered as linear rigid rotors.

In the diatomic molecule, the rotational energy depends on the moment of inertia of the system I where it is equal,

$$I = \mu R^2 \quad \text{..... (2.25)}$$

Where μ is the reduced mass of the molecule and R is half the distance between the two atoms.

According to Schrödinger equation:

$$\hat{H}\,\psi = E\psi \quad \text{..... (2.26)}$$

Where $\hat{H}$ is the Hamiltonian energy operator, ψ is the wave function, and E is the corresponding energy. In the free space, the energy operator corresponds to the system kinetic energy, [31] so

$$\hat{H} = -\frac{\hbar^2}{2\mu}\,\nabla^2 \quad \text{..... (2.27)}$$

Where $\hbar$ reduced Planck constant and ∇^2 is the Laplacian. The energy operator can be rewritten in terms of the spherical polar coordinates as following,

$$\hat{H} = -\frac{\hbar^2}{2I}\left[\frac{1}{\sin\theta}\frac{\partial}{\partial\theta}\left(\sin\theta\,\frac{\partial}{\partial\theta}\right) + \frac{1}{sin^{\,2}\theta}\frac{\partial^2}{\partial\varphi^2}\right] \quad \text{..... (2.28)}$$

The eigenvalue equation of the last equation is,

$$\widehat{H}\, Y_l^m(\theta,\varphi) = \frac{\hbar^2}{2I}\, l(l+1) Y_l^m(\theta,\varphi) \quad \text{..... (2.30)}$$

Where $Y_l^m(\theta,\varphi)$ is a set of functions (spherical harmonics). So the energy can be expressed as following,

$$E_l = \frac{\hbar^2}{2I}\, l(l+1) \quad \text{..... (2.31)}$$

Let $B = \frac{\hbar^2}{2I}$ where B is the rotational constant, we write,

$$E_l = B\, l(l+1) \quad \text{..... (2.32)}$$

In case of linear rotor, the selection rule $\Delta l = \pm 2$, the degeneracy is $2l + 1$, so that the shift of rotational Raman lines relative to the Rayleigh line can be written as,

$$\Delta\nu_{rot} = \pm B[(l+2)(l+3) - l(l+1)] = \pm B[4l+6] \quad (cm^{-1}) \text{.. (2.33)}$$

(±) sign refers to the position of the line on the right or on the left of the primary line. Therefore, the first rotational Raman line ($l = 0$) will appear after a separation of amount,

$$\Delta\nu_{rot} = \pm B[0+6] = \pm 6B \quad \text{..... (2.33)}$$

All the other lines will be separated a part of amount $4B$ with each other

(See figure 2.8).

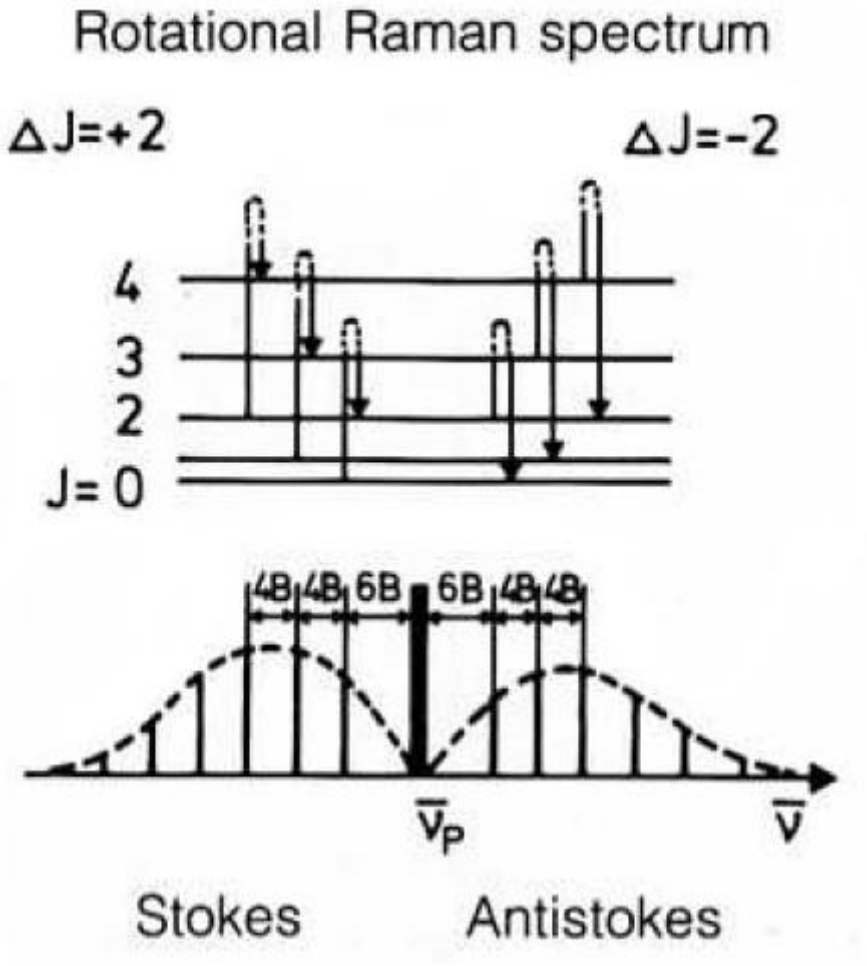

Figure 2.8. A diagram explaining the rotational Raman lines. [27]

2.4 The Quantum Agreement with the Classical Theory and Experimental Data

Using the wave mechanics, we can prove that there is agreement to between the quantum theory, classical theory and the experimental data. If there is a transition due to Raman scattering between two states *n* and *m*. the scattering moment can be given by

$$[P]^{nm} = \int \psi_n^* P \psi_m dr \text{ .... (2.34)}$$

Where ψ_n and ψ_m are the associated wave functions with the two states. By substituting the value of *P* under the integral from equation 2.5, we will notice that ψ_n^*, ψ_m, and P have time exponential parts. In addition, $[P]^{nm}$ will vary with a frequency $\nu_o + (E_n - E_m)/h$. Therefore, we can rewrite the last equation for the amplitude as following

$$[P^0]^{nm} = E \int \psi_n^* \alpha\, \psi_m dr \text{ .... (2.35)}$$

From the last equation, it is clear that the transition between the two energy states E_n and E_m will happen, after the scattering of the incident light of frequency ν_o resulting a scattered light of frequency $\nu_o + (E_n - E_m)/h$, if the integral is non-zero. To calculate the intensity of the corresponding Raman lines, we need to find the probability which is the square of the amplitude stipulated in the last equation giving a quantitative agreement of the quantum explanation and the experimental data.

If the polarizability in equation (2.35) is constant, so we can take it out of the integral giving

$$[P^0]^{nm} = E\alpha \int \psi_n^* \ \psi_m dr \text{ .... (2.36)}$$

Since ψ_n and ψ_m are orthogonal, the above integral will vanish except if *n* = *m* giving the Rayleigh line, i.e. at constant polarizability, we will get Rayleigh

scattering process but if the polarizability changes, Raman lines will appear. The last conclusion agrees with both the classical theory and the experimental data.

Chapter 3 RAMAN SPECTROSCOPIC STUDIES OF HYDROGEN CLATHRATES

3.1 Introduction

There are numerous means to study the hydrogen hydrates like X-ray diffraction, IR, neutron scattering and Raman spectroscopy. Our concern here is to study hydrogen hydrates using Raman spectroscopy. Raman spectroscopy can provide information regarding the vibrational and rotational bands of enclathrated hydrogen.

3.2 Analysis of the Rotatinal Modes using Raman Spectroscopy

Raman spectrum reveals the pure rotational transition of the compound. Pure rotational transitions can be described with the notation $S_o(J)$, with J = 0, 1, 2,….etc. The rotational transitions (rotons) are controlled by a selection rule to allow the transition, otherwise, it will be forbidden. This selection rule comes from the wave function constraints. In the Raman scattering, the selection rule for rotational transitions is $\Delta J = 0, \pm 2$ while the transition $\Delta J = \pm 1$ is forbidden in Raman scattering although it is allowed in IR rotational transitions. [32]

The occurrence of the rotational transition depends on the population of particles in the energy level. Therefore, at room temperature, we expect to have many transitions like $S_o(0)$, $S_o(1)$, $S_o(2)$, and $S_o(3)$ for H_2 molecule. They are closely equal separated. The same transitions appear for D_2 molecule but with additional $S_o(4)$ at room temperature. The fifth band of D_2 arises due to the increases mass (small rotational constant). Furthermore, D_2 bands are shifted to a lower frequency by a factor of two due to the mass ratio. The intensities of

the lines depend on the nuclear spin in addition to the population of the energy levels. Figure 3.1 shows the comparison between the rotational transitions of H_2 gas and D_2 gas at ambient standard temperature/ pressure (STP) conditions.

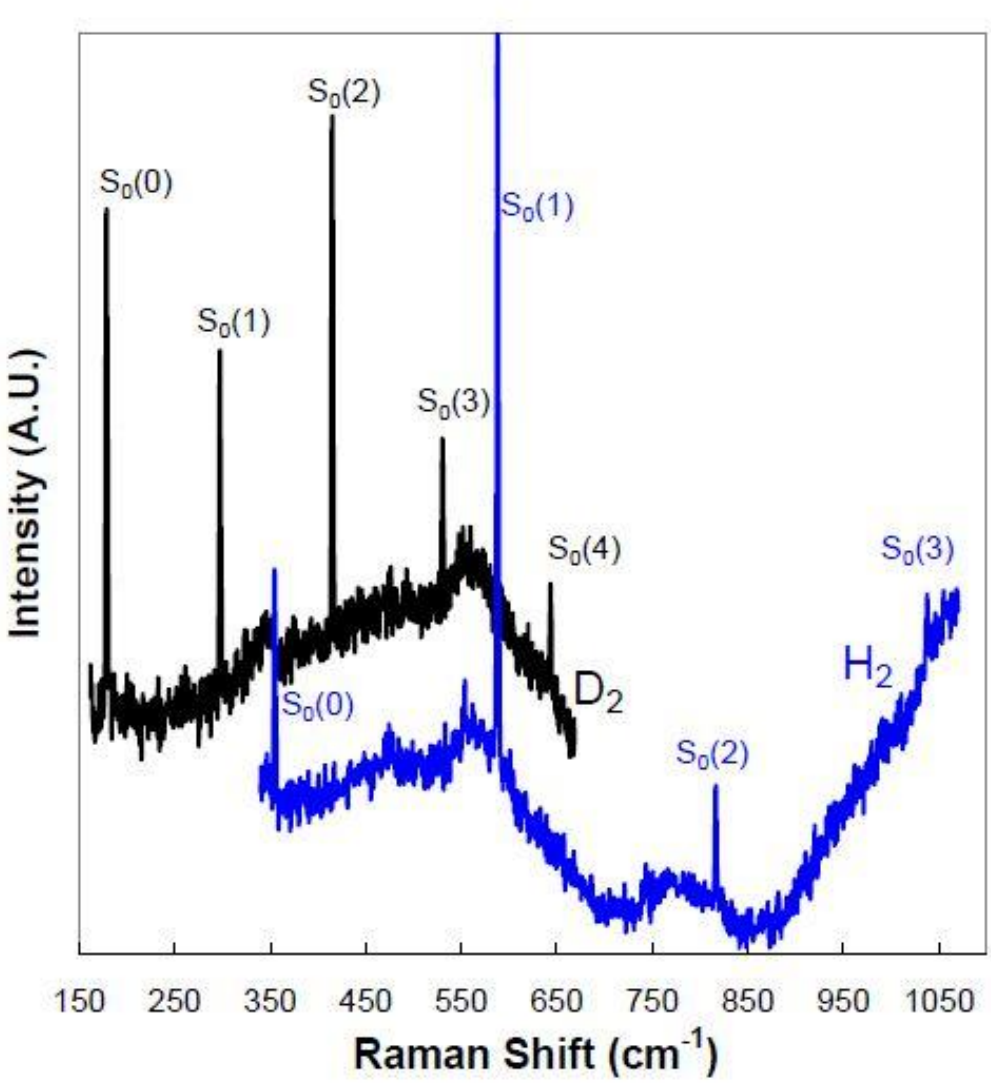

Figure 3.1. Raman spectra for rotons of H_2 gas (blue solid line) at the bottom and D_2 gas rotons (black solid line) at STP. [33]

For H_2, as temperature decreases down to 77 K, the population of the higher rota-tional level decreases. As a result, only $S_o(0)$ and $S_o(1)$ rotational transitions appear and others vanish. $S_o(0)$ appears at 354 cm^{-1} with a transition ($\Delta v = 0, J = 0 \rightarrow 2$, *para*-$H_2$). In addition, $S_o(1)$ is observed at 587 cm^{-1} with a transition ($\Delta v = 0, J = 1 \rightarrow 3$, *ortho*-$H_2$). In the clathrate phase,

these bands are widely broadened and their positions are slightly shifted to lower frequencies that are quite close to those of the free gas state which indicating that the trapped H_2 inside the clathrate undergoes nearly free rotation within a confining space. The rotational Raman spectral lines for H_2 gas at 0.1 MPa and 295 K and H_2 + THF (tetrahydrofuran) formed at 50MPa and 250 K, measured at 0.1 MPa and 76 K are shown in figure 3.2.

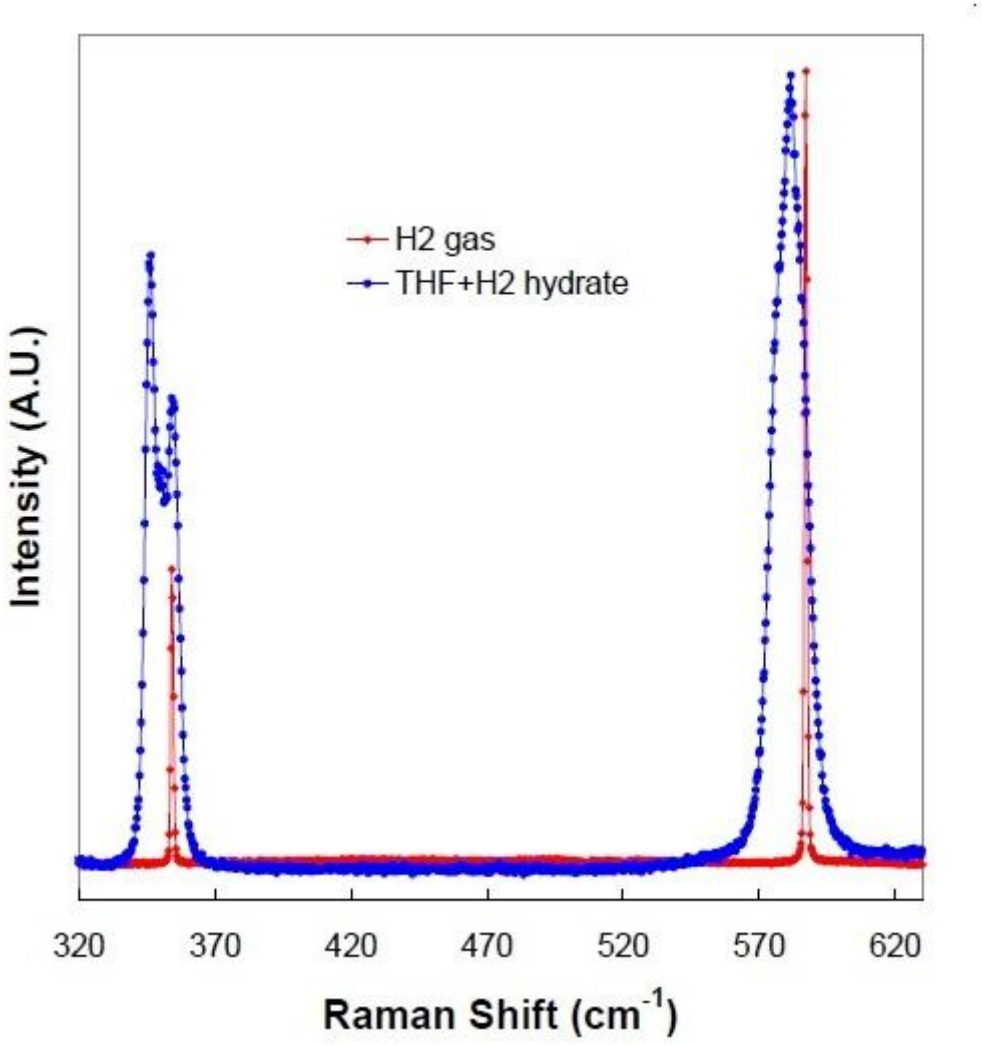

Figure 3.2. Rotational Raman spectrum for H_2 gas and H_2 + THF hydrate. [33]

For H_2 gas, from section (2.3) above, the rotational energy states are degenerate with a value of $2J + 1$. The degenerate levels of J can be divided into sub-levels of using the second quantum number *m*. *m* can take values from $J, J-1,\ J-2, \ldots\ldots, -J$. At $J = 0$, so *m* will equal zero too meaning that the spherical harmonics probability density will be a sphere, therefore, it doesn't depend on the orientation. At $J = 1$, *m* can take values 1, 0, -1. This makes the spherical harmonics probability density to be flattened or elongated spheroids. [34] For all values of *m*, the energy levels are equal in terms of energy and this affect the population which, in turn, affects the intensity of the Raman spectral lines.

Since hydrogen suffers from strong interaction with water to form the clathrate, so the degeneracy may be completely lifted and, hence, there will be five possibilities for the Raman transition ($J = 0 \rightarrow 2$) of *para*-H_2 to move from $J = 0$, *m* = 0 to one of the five different *m* ($J = 2$, *m* = 2, 1, 0, -1, -2). However, we find three transitions only resolvable in figure 3.3.

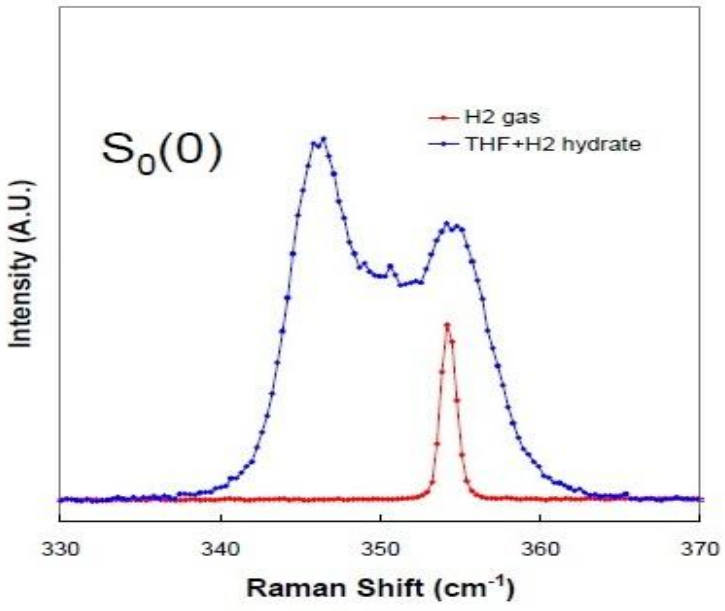

Figure 3.3. Rotational transitions of H_2 in H_2+THF (blue line). [33]

.

According to recent theoretical calculations for one H_2 molecule trapped in the small cavity, it is proven that there are five transitions from $J = 0, m = 0$, to sub-levels of $J = 2, m = 2, 1, 0, -1, -2$. They appear at 348.6, 349.6, 356.0, 363.4, and 364.3 cm^{-1}. [28] We can notice that the energy difference between the first and the last two lines is small. Therefore, we cannot detect the five transitions and we, instead, observe only three.

In case of *ortho*-H_2, we cannot detect individual transitions because of the large number of possibilities accompanied by small energy differences.

In case of simple hydrogen hydrate, there are hydrogen molecules captured in the small and large cages. To find the rotational Raman line, it is a superposition of *ortho*-H_2 and *para*-H_2 in both small and large cages. In 2011, Giannasi et al. did a research to study the share of individual small and large cages. [35] Giannasi et al. assumed that the small cages are occupied with one hydrogen molecule in both simple and binary clathrate hydrates. Therefore, the contribution of the small cages will be the same in the output rotational transitions. Giannasi et al. prepared binary clathrate of H_2+THF. The THF occupies the large cages in the binary clathrate hydrate. They obtained the $S_o(0)$ and $S_o(1)$ for THF and subtracted the output signal from the spectrum of simple hydrogen hydrate to obtain the contribution of the hydrogen in the large cages only.

To evaluate the amount of hydrogen occupying the small and large cages, Giannasi et al. analyzed the intensity of the separate contribution. They found that 40% of H_2 occupy the large cages, while the remaining 60% occupy the small cages. They confirmed their results using the vibrational spectrum.

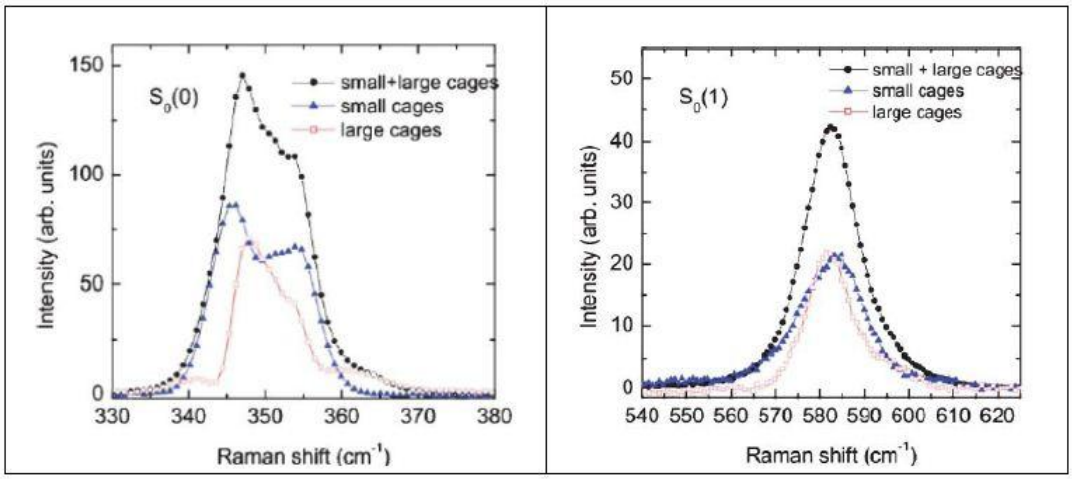

Figure 3.4. *Para-* and *ortho-* hydrogen showing the individual contribution of small and large cages. [35]

3.2.1 *Ortho-Para* Conversion

The overall wavefunction of the molecule is the product of the spatial functions and the spin functions. Exchange of the nuclei means inversion in space. Under this condition, the odd rotational eigenfunctions $J = 1, 3, 5, ...$ will change their sign, so they have negative parity and are anti-symmetric. On the other hand, the even eigenfunctions $J = 0, 2, 4, ...$ will have the same sign under the inversion in space; therefore, they have positive parity and are symmetric. Full details regarding the parity of the overall wavefunction, spatial function, and spin function of H_2 is explained in figure 3.5.

Unlike the H_2, D_2 is a considered a boson not a fermion with integer spin making the overall parity of the wavefunction to be positive and symmetric. Thus, *ortho*-D_2 can have spin $I = 0, 2$ can appear only with even rotational states (statistical weight 2) while D_2 can have $I = 1$ in the case of odd rotational states (statistical weight 1).

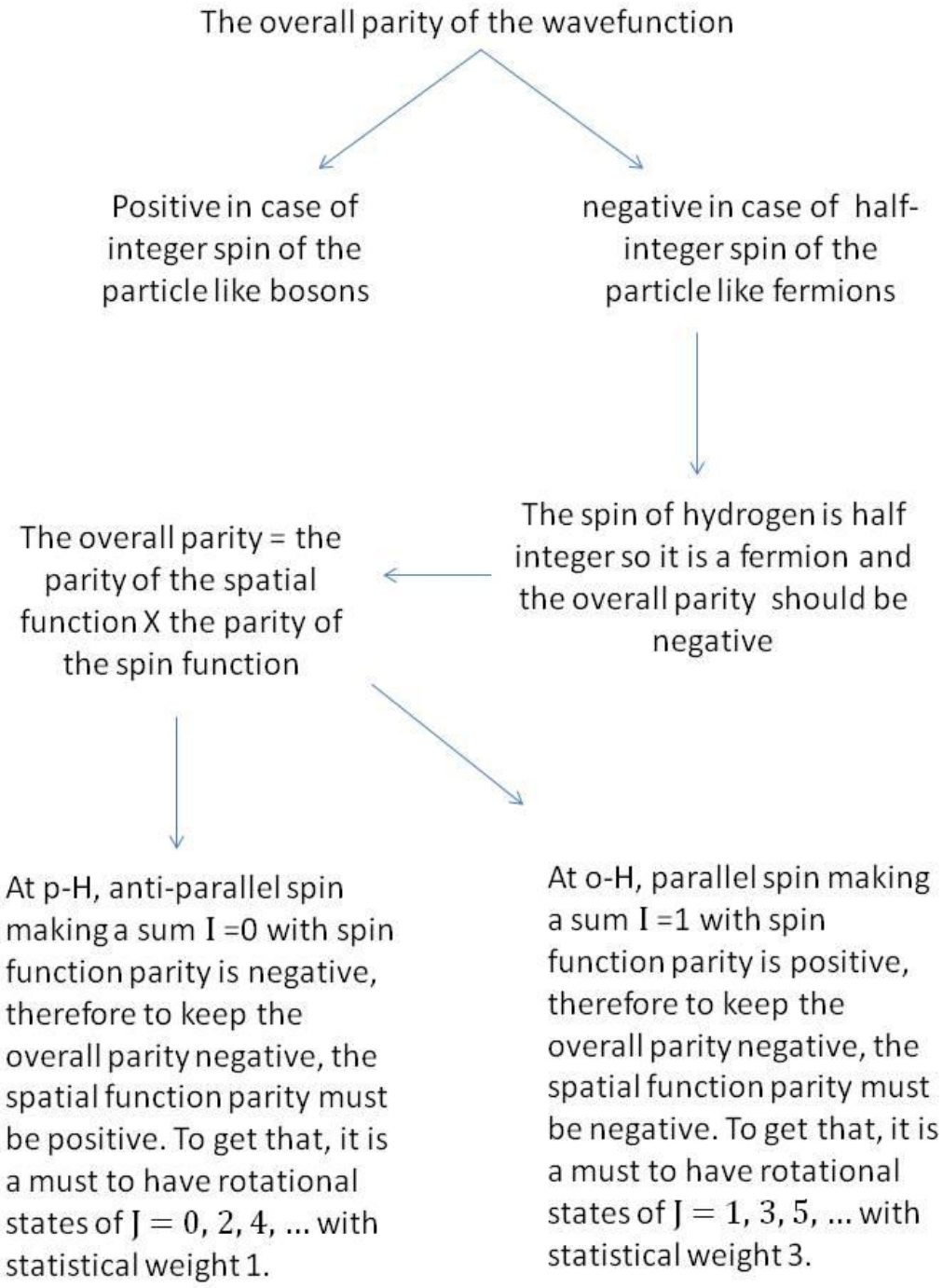

Figure 3.5. A schematic diagram to show the constraints of the rotational states in *ortho* and *para*-H_2.

For a diatomic molecule, From section 2.3, the rotational energy, $E(J)$, can be expressed as following

$$E(J) = BJ(J+1) \quad \text{..... (3.1)}$$

Where B is the rotational constant (59.322 cm^{-1} for H_2 in the ground level and 29.904 cm^{-1} for D_2) and J is the rotational quantum number. Both *ortho* and *para*-H_2 exist at the same time. The ratio between them is a function of temperature. The ratio can be expressed as

$$\frac{n^o}{n^p} = 3\frac{\sum_{J=odd}(2J+1)e^{-\beta E(J)}}{\sum_{J=even}(2J+1)e^{-\beta E(J)}} \quad \text{..... (3.2)}$$

Where $\beta = 1/k_B T$, $2J+1$ is the degeneracy of the rotational states and factor of three due to the statistical weights. $k_B$is the Boltzmann constant.

At high temperature,

$$T \gg \frac{Bhc}{k_B} \quad \text{..... (3.3)}$$

The ratio of *ortho* to *para* decreases to the ratio of the statistical weights (3:1 for H_2, and 2:1 for D_2) because the high temperature makes the molecules more energetic and hence the conversion occurs easily. Figure 3.6 shows the equilibrium percentage of *ortho* and *para* for both H_2 and D_2 with changing the temperature. Because of the low rotational constant for D_2, the *ortho-para* conversion ratio deviates at low temperature than H_2 from the normal ratio.

Giannasi et al. [36] introduced a new equation to determine the relative population of *para*-H_2 from the rotational spectral lines $S_o(0)$ and $S_o(1)$, which is given by

$$\frac{I_{s_0}}{I_{s_1}} = \frac{b_{02}}{b_{13}}\frac{\gamma_0^2}{\gamma_1^2}\frac{v_0^3}{v_1^3}\frac{X_p}{1-X_p}\frac{P_0}{P_1} \quad \text{..... (3.4)}$$

Where

I_{s_0}: The area under S_0 (0), while I_{s_1} stands for the area under S_0 (1)

b_{02}: The statistical weight for transition from 0 to 2, and the same for b_{13}.

γ_i : The polarization anisotropy for the initial energy state

υ : the frequency of the scattered radiation

P_0 : The parahydrogen population at energy state $J = 1$

P_1 : The orthohydrogen population at energy state $J = 2$

In the clathrate hydrate, the self-conversion process in the small cages takes a long time than the large cages because the clathrate isolates the trapped molecule from the extrinsic effect of the surroundings. Generally, the trapped molecules undergo self-conversion slower than the free gas because the clathrate cavities reduce the extrinsic effects which are responsible for flipping the nuclear spin. [36] Figure 3.7 shows the concentration of *para*-H_2 with time for simple and binary clathrate hydrate.

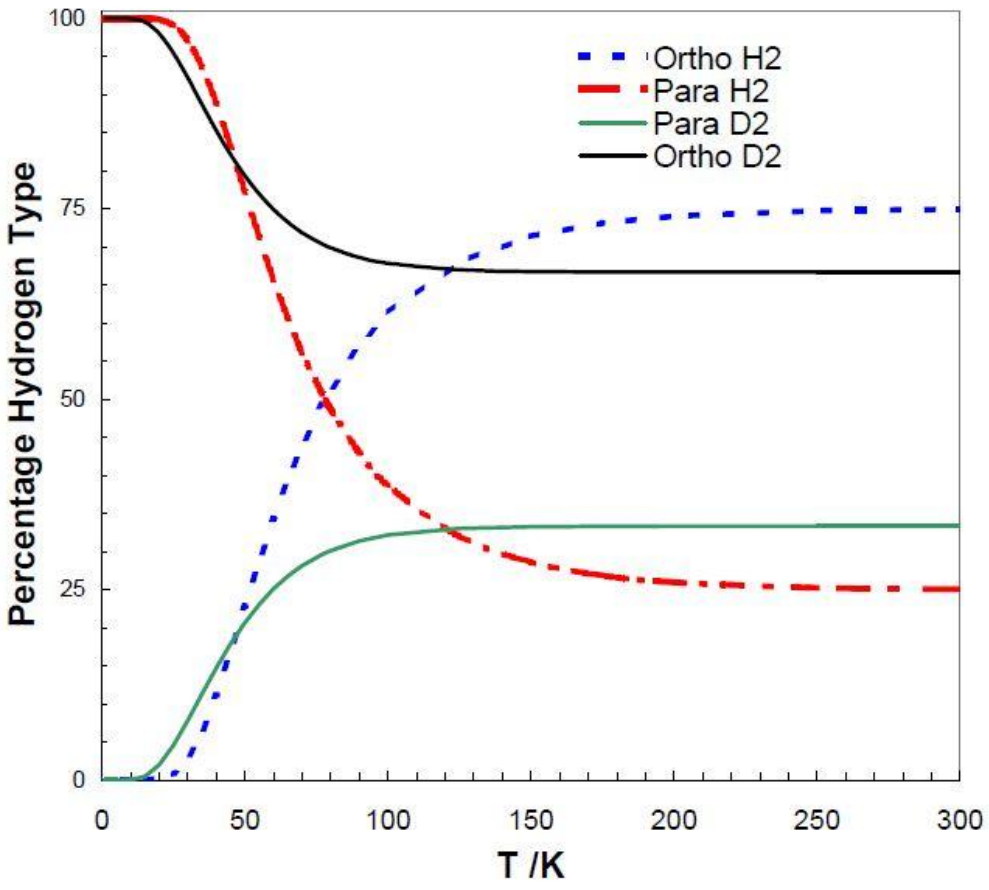

Figure 3.6. Shows the equilibrium percentage of *ortho* and *para* for both H_2 and D_2 with changing the temperature. [33]

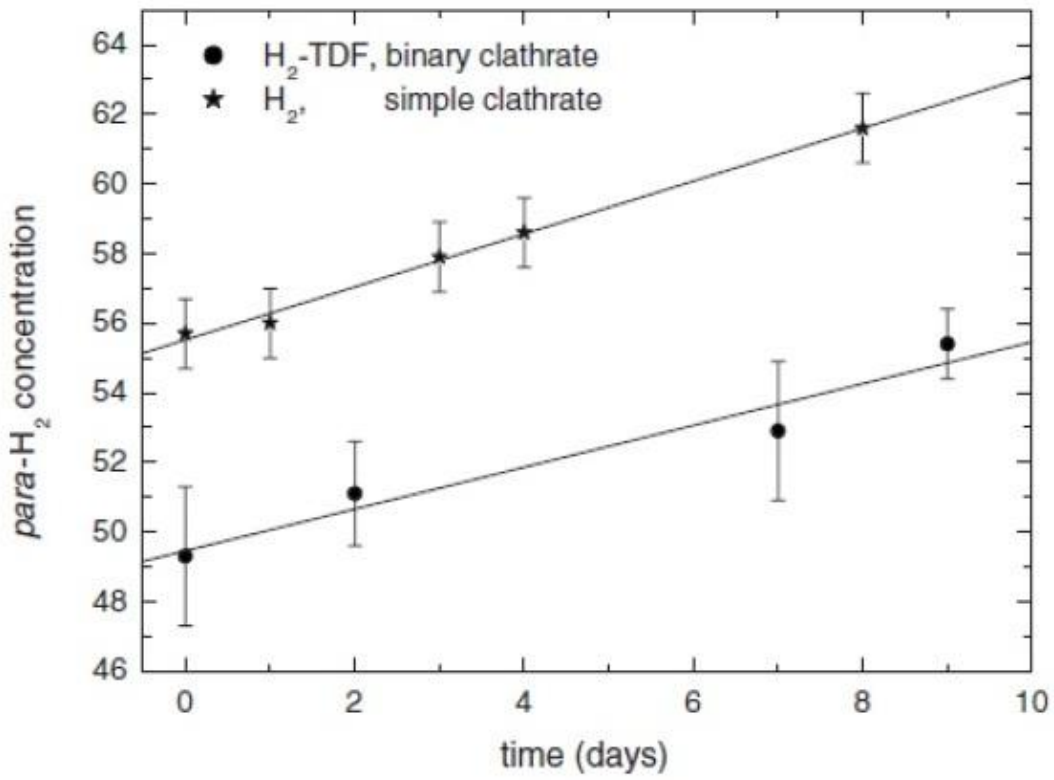

Figure 3.7. Shows the concentration of *para*-H_2 with time for simple and binary clathrate hydrate. [36]

3.3 Analysis of the Vibrational Modes using Raman Spectroscopy

Raman spectrum, as we explained before, has both vibrational and rotational transitions. The rotational transitions have been studied in the last section, so our concern will be studying the vibrational bands. Vibrational transitions with no rotational transition (i.e. $\Delta J = 0$) occurs from the ground state to an excited state are called Q transitions. Quantum mechanically, the energy of different energy states can be given by

$$E_n = \left(n + \frac{1}{2}\right) h\nu \quad \text{..... (3.5)}$$

Where n is the vibrational quantum number and its selection rule $\Delta n = n \rightarrow n'$ (in this research it is always 1), h is the Planck constant and ν is the frequency. To identify a specific vibrational transition, we can use the notation $Q_{\Delta n}(J)$ where J is the rotational quantum number.

3.3.1 Vibrational Modes of H_2

H_2 gas at room temperature has obvious four vibrational lines labeled $Q_1(0)$, $Q_1(1)$, $Q_1(2)$ and $Q_1(3)$. The intensity of the second transition is large because of the *ortho-para* ratio and by the rotational population. [37] Figure 3.8 shows the four vibrational lines of H_2 gas at room temperature and 1 bar.

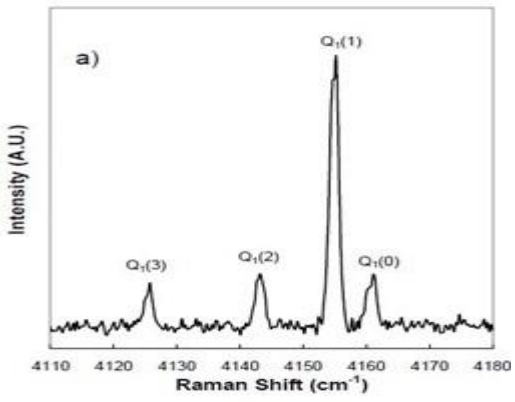

Figure 3.8. H_2 vibrational Raman spectrum at room temperature and 1 bar. [33]

As the temperature decreases, the population of higher rotational energy levels decreases reducing the observed vibrational transitions to two only instead of four. The lines are $Q_1(0)$ and $Q_1(1)$ and they represents transitions from $\nu = 0,\ J = 0 \rightarrow \nu = 1,\ J = 0$ (*para*-H_2) and $\nu = 0,\ J = 1 \rightarrow \nu = 1,\ J = 1$ (*ortho*-H_2) respectively. The separation between them is 6 cm^{-1} in the H_2 fluid at 76 K. The hydrogen molecule trapped inside a cavity will show the same two lines but down shifted from the free gas lines due to the applied potential that molecules experience inside the cage. [19] In addition, we can find that as, the size of the cage differs, or, the occupancy of a cage changes, the vibrational lines frequencies of the trapped H_2 changes too. For example, if we have singly occupied small cages, they will show two spectral lines (*ortho* and *para*) down shifted from those of the free gas, however, if we have doubled occupied cages, they will give two spectral line in a different region than the small cages or the free gas.

The assignment of the spectral lines to specific occupancy number and a specific cage is challenging. The hydrogen has two spectral lines with a difference between them around 6 cm^{-1}. Each certain occupancy in a definite cage will give these two lines. The small cage can hold one molecule giving two spectral lines and their positions are separated from those of molecules in the large cavity. The assignment becomes more complicated for the large cage. There are cages with one, two, three, or four hydrogen molecules giving many spectral lines that overlap together. The difficulty of the assignment process increases as we take into account; the *ortho-para* conversion with time, and, the change of the large cage occupancy with the temperature and pressure changes.

In sII clathrate, there are small cages and large cages. In 2002, Mao et al. assigned the two lowest frequency peaks to hydrogen in the large cage and the others to hydrogen in the small cages. [13]

However, in 2007, Strobel et al. has proven that the two lowest frequency peaks are assigned to the hydrogen in the small cage not the large cage, and the

other three lines to hydrogen in the large cage not the small. [37] Strobel et al. prepared a binary clathrate hydrate (H_2+THF) at 150 MPa and 250 K. In this situation, the THF molecule occupies the large cavity so; the Raman spectral line of the clathrate will be due to the hydrogen in small cavities only. In addition, they formed a pure H_2 hydrate at 150 MPa and 250 K. This hydrate will show hydrogen Raman spectral lines of both small and large cages. Figure 3.9 compares Raman spectra for pure H_2 fluid, binary THF+H_2 and pure H_2 hydrate measured at 76 K and atmospheric pressure. The pure and binary sII hydrates have an intense line at 4120 cm^{-1} and a shoulder at 4125 cm^{-1}. Unlike the binary sII hydrate, the pure hydrate has other three lines. Therefore, they must belong to hydrogen in the large cage, as this cage is filled with THF in the binary hydrate. Thus, the assignment is the reverse of Mao et al. suggestion.

The free H_2 gas consists of 75% *ortho*-H_2 and 25% *para*-H_2. After the synthesis of the clathrate, the vibrational line will show the same *ortho* to *para* ratio but, as time passes, this ratio changes because the conversion takes place.

Strobel et al. confirmed the *ortho-para* conversion. They take an immediate measurement of Raman spectrum for the binary clathrate hydrate (H_2+THF) after synthesis at 0.1 MPa and 76 K. They compared the resulted spectrum with the spectrum of another measurement for the same material after six days of storage at liquid N_2. *ortho* to *para* conversion happened and *para*-H_2 becomes the dominant. Figure 3.10 shows the *ortho* to *para* conversion for H_2 at H_2+THF binary clathrate.

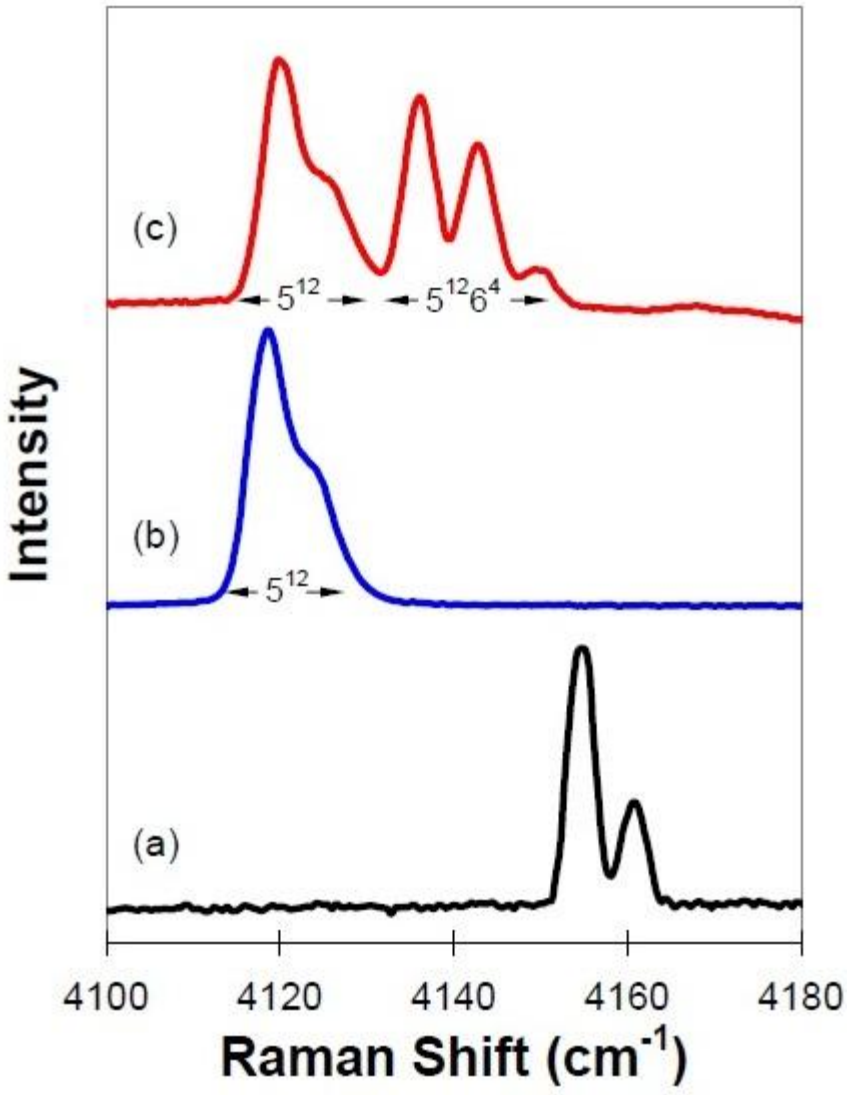

Figure 3.9. Raman spectrum at 76 K and atmospheric pressure for: (a) H_2 gas, (b) H_2+THF and (c) hydrogen hydrate. Both hydrates were formed at 150 MPa and 250 K. [33]

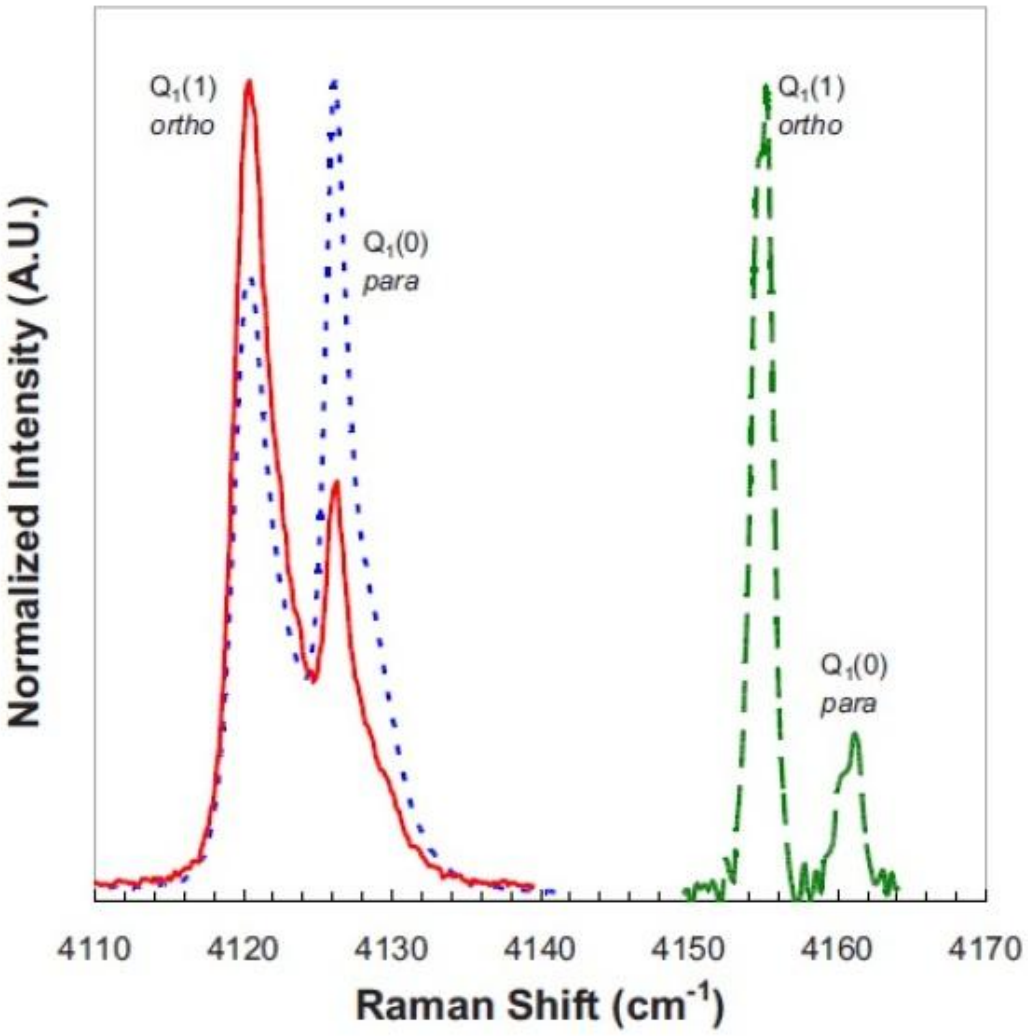

Figure 3.10. Vibrational Raman spectrum for free H_2 gas at 0.1 MPa and 296 K (dashed green curve), H_2+THF at 0.1 MPa and 76 K after the synthesis directly (solid red curve), and for the same sample after 6 days of storage in liquid N_2 (dotted blue curve). [33]

To specify the spectral peaks, measured at 76 K produced from hydrogen trapped inside a sII structure of clathrate hydrate formed at 200 MPa and 250 K, to definite occupancies, Strobel et al. [8] assumed that there is one hydrogen molecule in the small cages and large cages are filled with two (2L), three (3L), or four molecules (4L). Therefore, we must have eight lines but some of them may overlap. To get more resolution, we can heat the sample up to 150 K and cool it again to 76 K. Figure 3.11 shows the resulted Raman spectrum of simple H_2 hydrates after many heat/quench cycles.

After the first heat/quench cycle, it is clear that the 4L intensity decreased meaning a loss of the hydrogen while the intensity of 3L aroused. With one more heat/quench cycle, double occupied large cages population started to increase. The fourth heat/quench cycle makes the 4L to completely dissociated.

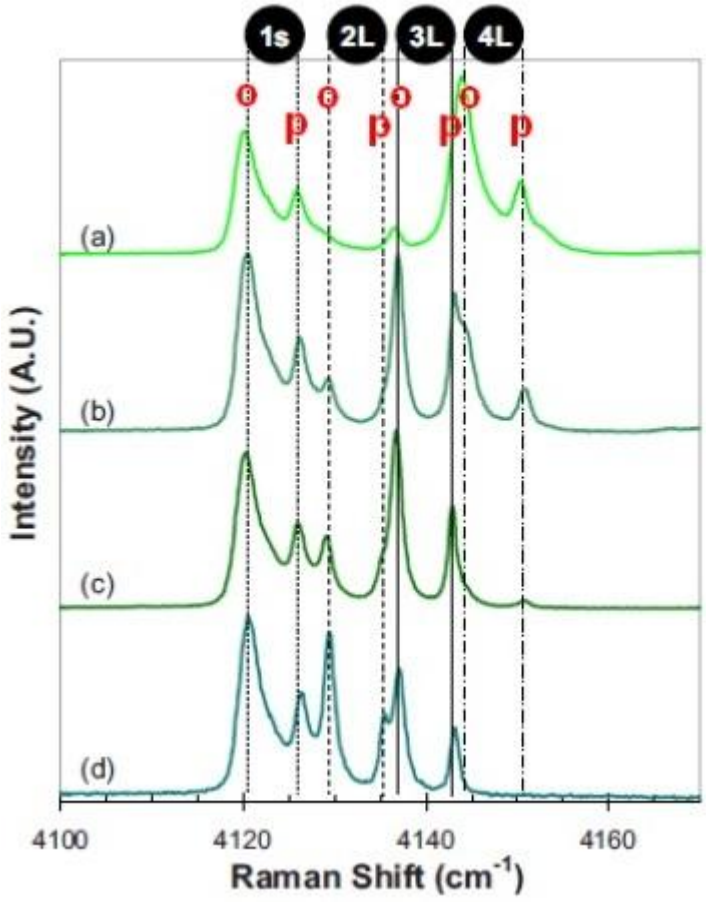

Figure 3.11. Vibrational Raman spectra for simple H_2 hydrate. Curves (a), (b), (c), and (d) are the vibrational spectral curves after heating the sample to 150 K and cooling to 76 K repeatedly. [33]

On the other hand, Giannasi et al. [36] proposed a different assignment of peaks to cages population. They suggested that small cages are filled with one molecule of H_2 while the large cages can be occupied with one (1L), two (2L), and three (3L) molecules. Therefore, we must have eight spectral components in the Raman spectrum. Figure 3.12 shows a comparison between the Raman measurements for H_2 hydrates: one obtained after the formation of the clathrate and the other after three months storage at low temperature.

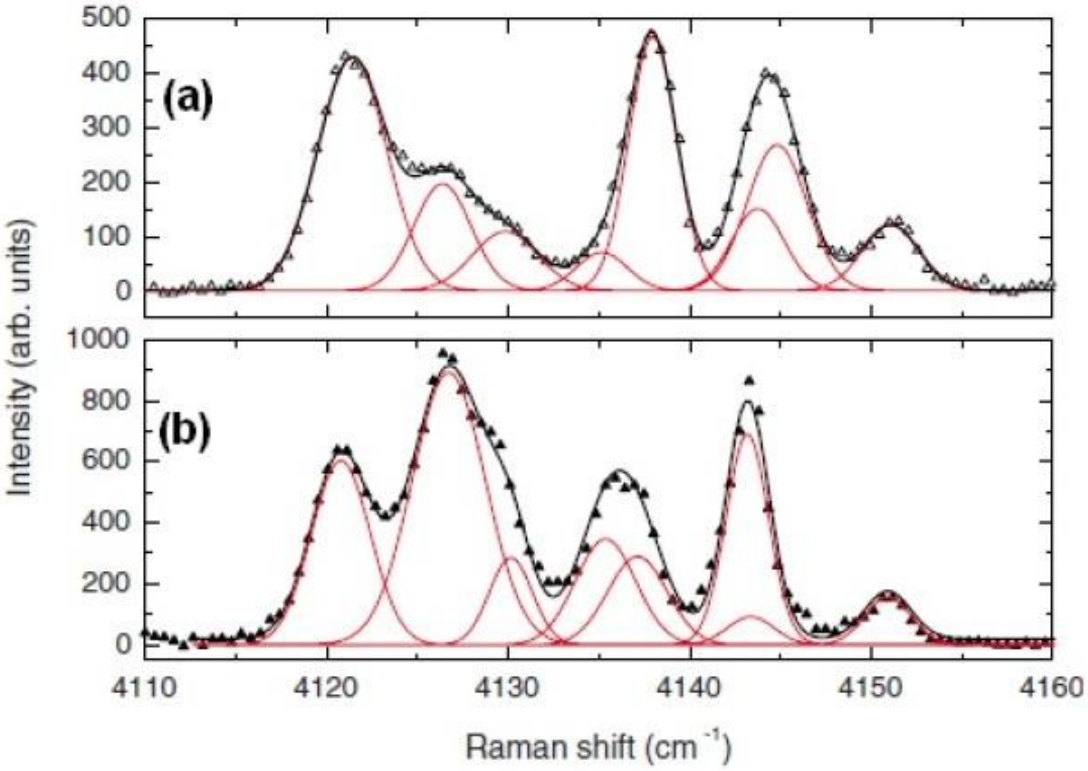

Figure 3.12. Two Gaussian fitted Raman spectra: (a) spectrum obtained at 77 K after the formation of the hydrate. (b) spectrum obtained at 77 K after three months storage in low temperature. [36]

3.3.2 Vibrational Modes of D_2

D_2 gas at room temperature has five vibrational transitions $Q_1(0)$, $Q_1(1)$, $Q_1(2)$, $Q_1(3)$, $Q_1(4)$. The figure 3.13 shows the D_2 vibrational transitions at room temperature. The intensity of the third transition is large because of the *ortho-para* ratio and by the rotational population. By comparing the figure 3.8 with figure 3.13, it clear that the D_2 vibration bands appear at lower frequencies than H_2.

As the temperature decreases, the population of higher rotational energy levels decreases reducing the observed vibrational transitions to three only instead of five. The lines are $Q_1(0)$, $Q_1(1)$, and $Q_1(2)$ representing transitions from $v = 0,\ J = 0 \rightarrow v = 1,\ J = 0$ (*ortho*-D_2), $v = 0,\ J = 1 \rightarrow v = 1,\ J = 1$ (*para*-D_2), and $v = 0,\ J = 2 \rightarrow v = 1,\ J = 2$ (*ortho*-D_2) respectively. Therefore, in normal D_2, the ratio of *ortho* to *para* is 2:1 although the rotational constant for D_2($B \sim 30$ cm^{-1}) is about half of that H_2 ($B \sim 60$ cm^{-1}). Figure 3.14 shows the three vibrational transitions for enclathrated D_2.

For the D_2 hydrate, the frquency difference between the first two transitions is nearly two cm^{-1} ($Q_1(0) - Q_1(1) \sim 2$ cm $^{-1}$). The frequency difference between the last two transitions is nearly four cm^{-1} ($Q_1(1) - Q_1(2) \sim 4$ cm^{-1}). The D_2 molecule trapped inside a cavity will show the same three lines but down shifted from the free gas line.

The same procedure of how we have assigned the Raman vibrational peaks to definite occupancy per cage for H_2 will be applied for D_2 as well. Measuring the total Raman spectrum, then suggesting occupancies like 1S, 2L, 3L, and 4L if we followed Strobel et al. way (figure 3.15), or, 1S, 1L, 2L, and 3L if we follow Giannasi et al. way (figure3.16). After that, applying heat/quench cycles many times to get more resolved data and to verify the suggestion we used.

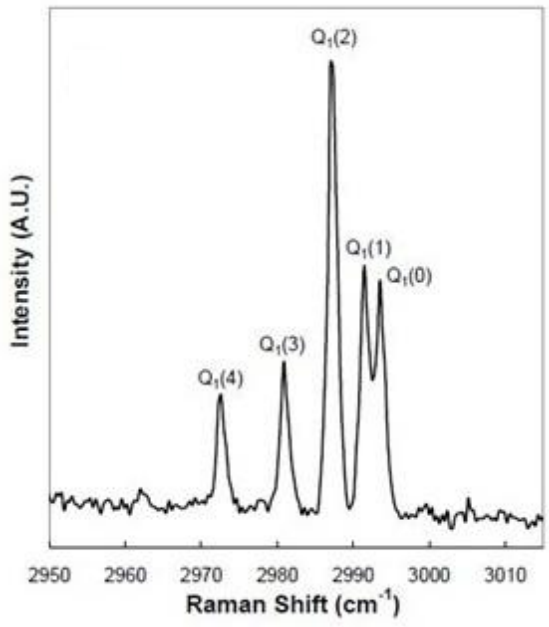

Figure 3.13. D_2 gas vibrational transition at room temperature. [33]

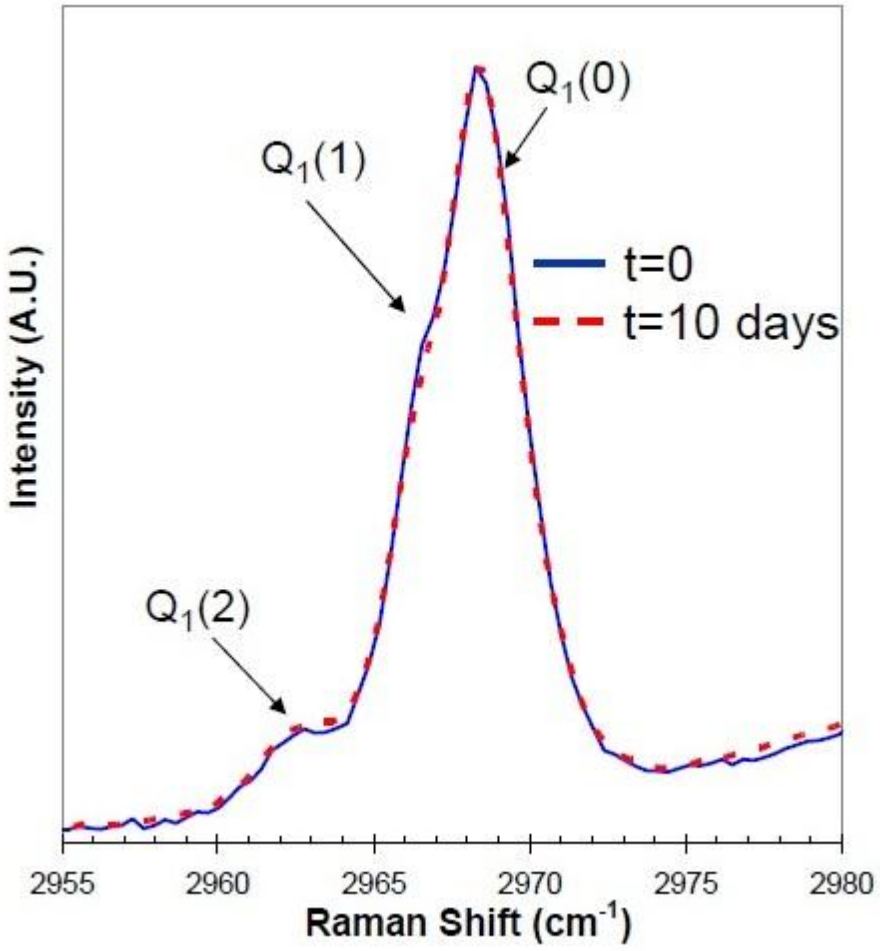

Figure 3.14. Shows the three vibrational transitions for enclathrated D_2+THF formed at 100 MPa and 265 K. Solid blue line is the Raman measurement directly after formation, dashed line is the Raman spectrum after 10 days storage in liquid nitrogen. [33]

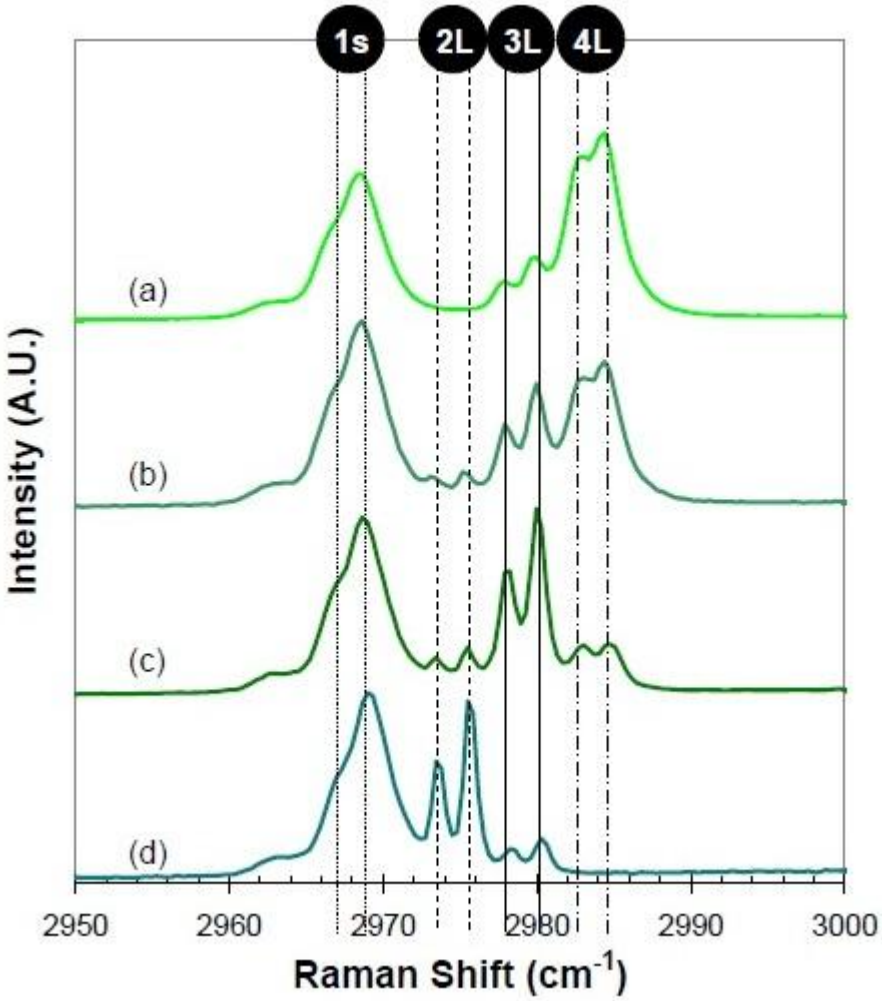

Figure 3.15. (a) vibron Raman spectrum of unperturbed D_2 hydrate formed at 192 MPa and 260 K, measured at 76 K and 0.1 MPa. (b)-(d) heat to 150 K / quench 76 K. Vertical lines indicates $\boldsymbol{ortho\ Q_1(0)\ and\ para\ Q_1(1)}$ contributions: 1 D_2/small cage (1s), 2 D_2/large cage (2L), 3 D_2/large cage (3L), 4 D_2/large cage (4L). $\boldsymbol{Q_1(2)}$ isn't labeled for clarity. [33]

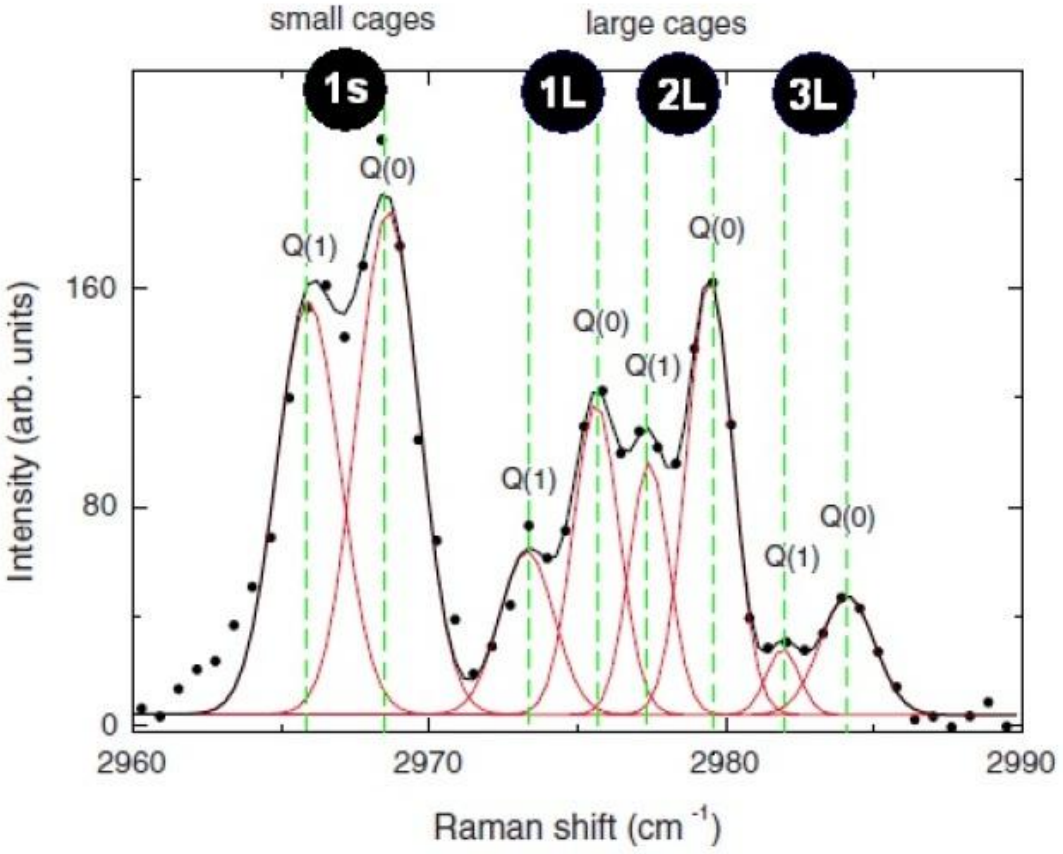

Figure 3.16. Fitted Raman spectrum with constrained eight Gaussian curves of D_2. The assignment of the large cage occupancy proposed by Giannasi et al. is shown. [36]

Chapter 4 THE EXPERIMENTAL PROCEDURE AND ANALYSIS OF RAMAN SPECTRUM OF SIMPLE sII DEUTERIUM CLATHRATE HYDRATES

As shown in the last chapter, there are two scopes for the assignment of the Raman peaks due to large cages to their prospective occupancy. Giannasi et al. [36] assigned the Raman peaks of deuterium in large cages to be filled with one (1L), two (2L), and three (3L) molecules. On the other hand, Strobel et al. [33] suggested that the large cages of simple deuterium hydrates could be filled with two (2L), three (3L) and four (4L). In this chapter, the experimental procedure and the analysis of Raman peaks with a new assignment of peaks will be introduced. This experimental part has been done in Raman Laboratory of Institute of Complex Systems in the National Research Center (CNR) at Sesto Fiorentino, in Italy.

4.1 Equipment and Experimental Procedure

The devices have been used in the experiment will be described in details in addition to the procedure itself. The experiment has the following components:

1. Argon laser (Coherent Innova 300)
2. Mirrors and lenses
3. Notch filter
4. Cell made from beryllium-copper alloy
5. Cryogenic system (helium closed cycle refrigerator)
6. Evacuating pump (Turbomolecular pump)
7. Barksdale pressure transducer
8. Pipelines
9. Nova-Swiss membrane compressor

10. Horiba Symphony Charge coupled device detector (CCD)
11. Telescope (made locally in CNR) connected to a television
12. Monochromator (Spex 1877 triple-mate spectrometer)
13. Temperature sensors

4.1.1 Setup of the Cell

To form the clathrate, we need a specific designed cell for this purpose. This cell must be connected to a gas source and bear gas pressure up to 3000 bar at a temperature range from 300 to 20 K. In addition, it must have an optical diamond window, to let the laser to fall on the sample, and to be collected after the scattering process. Moreover, the cell volume must be relatively small to be placed in the cryogenic system. To satisfy the last conditions, the cell material has been chosen to be beryllium-copper alloy (Berylco 25A bought from NGK Metals Corporation). This material is characterized by high thermal conduction coefficient in addition to very high yield strength. The cell shape is cylindrical with a diameter of 40 mm and a thickness of around 25 mm. Two or three drops of distilled water are placed in a container inside this cell. The surface of the distilled water is illuminated with the incident laser. The laser beam is incident at 90^{o} degree, therefore, we uses the back-scattering technique. This technique is preferred because it depends only on one window instead of two for any another configuration. The window of the cell must be clear, made from diamond in order to be transparent for the incident laser beam. In addition, the diamond window can afford up to 5000 bar without need to increase the thickness. Also, the window has a cylindrical geometry with a diameter 5.0 mm and a thickness 1.25 mm. By using a very thin layer of silicon glue, the window can be mounted to the clamping disk. This glue has no effect on the seal of the window. To make the cell withstand at very high pressure, a "Bridgman seal" can be used between the optical plug and the cell body. [34] In the Bridgman seal, we depend on a viscous material such as copper is set to

expand longitudinally against the increasing internal pressure. Full description of the cell components and dimensions are presented in figure 4.1.

To control the temperature of the cell, the cell is connected with a closed circuit refrigerator (CCR) (uses helium as cooling gas) able to cool the cell down to 10 K. In addition, the cell is embedded into a copper block for good thermal stability. To measure cryogenic temperatures, a silicon diode (Lakeshore DT 471) has been placed few millimeters away of the cell and in good contact with the copper block. A similar one must be connected to the cold finger of the cryostat. The difference between both sensors is always less than 2 K. A stainless steel capillary, welded to the cell, allows gas evacuation and transfer of deuterium (D_2). To get the required high pressure to the synthesis of deuterium clathrate, we use a Nova-Swiss membrane compressor that can provide a high pressure up to 3000 bar. Barksdale pressure transducer is used to measure the pressure up to 3500 bar. The CCR head and the sample holder are enclosed into a copper radiation shield. Finally, all are enclosed in a steel vacuum chamber equipped with a glass window. This steel vacuum chamber is evacuated from air and any other contaminating gases by a turbomolecular pump to 8.32×10^{-7} mbar. The overall system is mounted on a movable rack, which can be easily aligned with the optical system during spectroscopic measurements. Photographs of the cell and of its details are reported in figure 4.2. A photograph of the CCR mounted over a movable rack, controlled by wheels, is shown in figure 4.3. Figure 4.4 shows the Nova-Swiss membrane compressor. Lakeshore DT 471 is being used to measure the temperature of the cell device is shown in figure 4.5. The cryogenic system and its evacuating pump are shown in figures 4.6 and figure 4.7. Figure 4.8 shows the turbomolecular pump that evacuates the steel chamber from air down to 8.32×10^{-7} mbar.

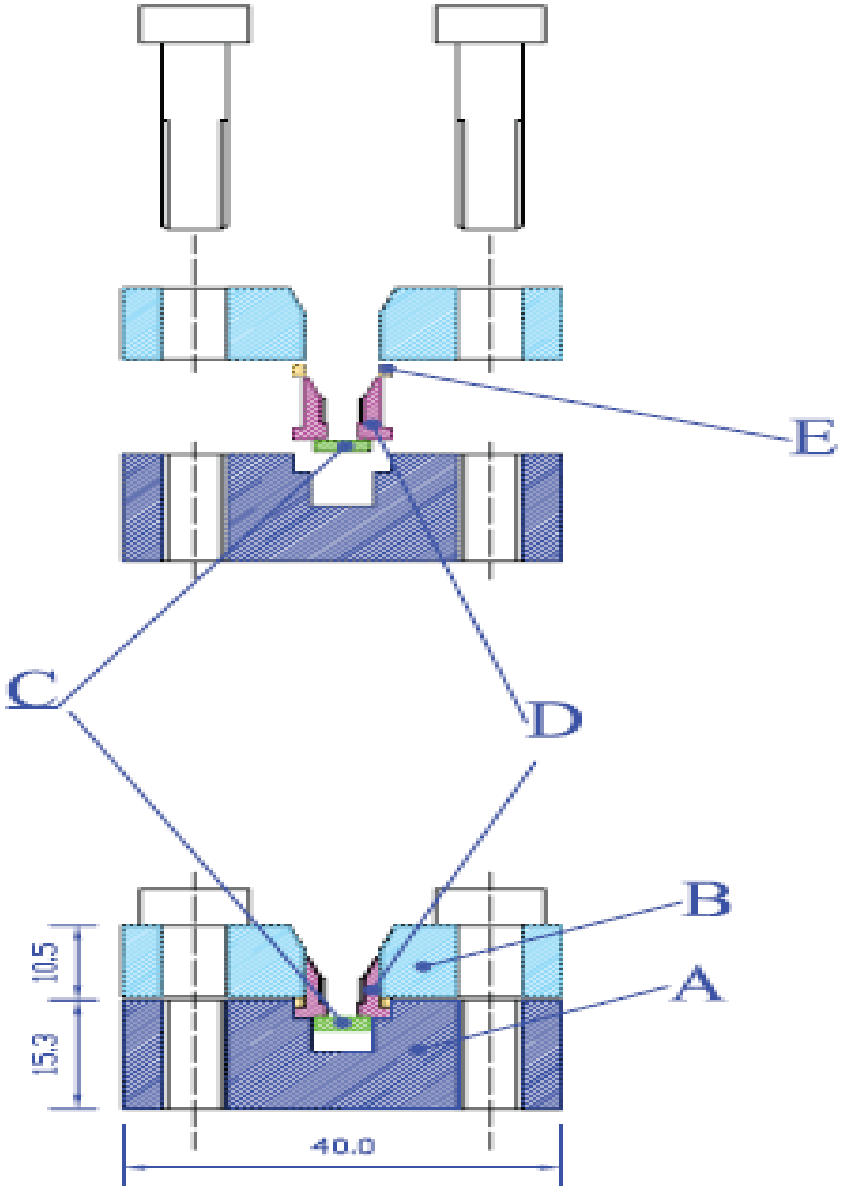

Figure 4.1. Schematic diagram of the dismounted cell (top drawing), and the mounted one (down drawing). The cell consists of (A) Cell body, (B) flange, (C) diamond window, (D) optical plug, and (E) pressing ring. [38]

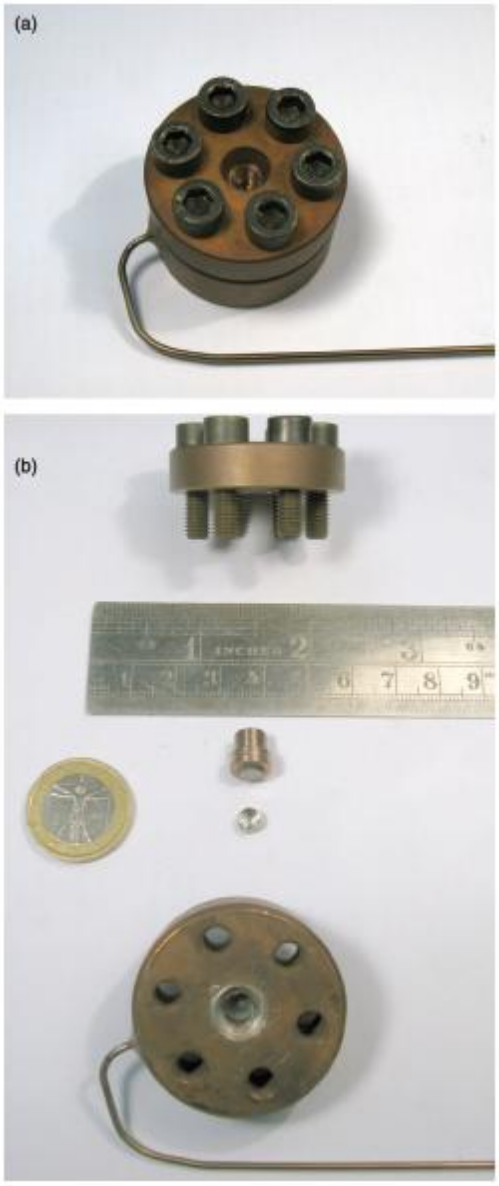

Figure 4.2. (a) Photograph of the mounted cell, (b) photograph of the dismounted cell. The pressing ring is still mounted on the optical plug where the glued diamond window is visible.

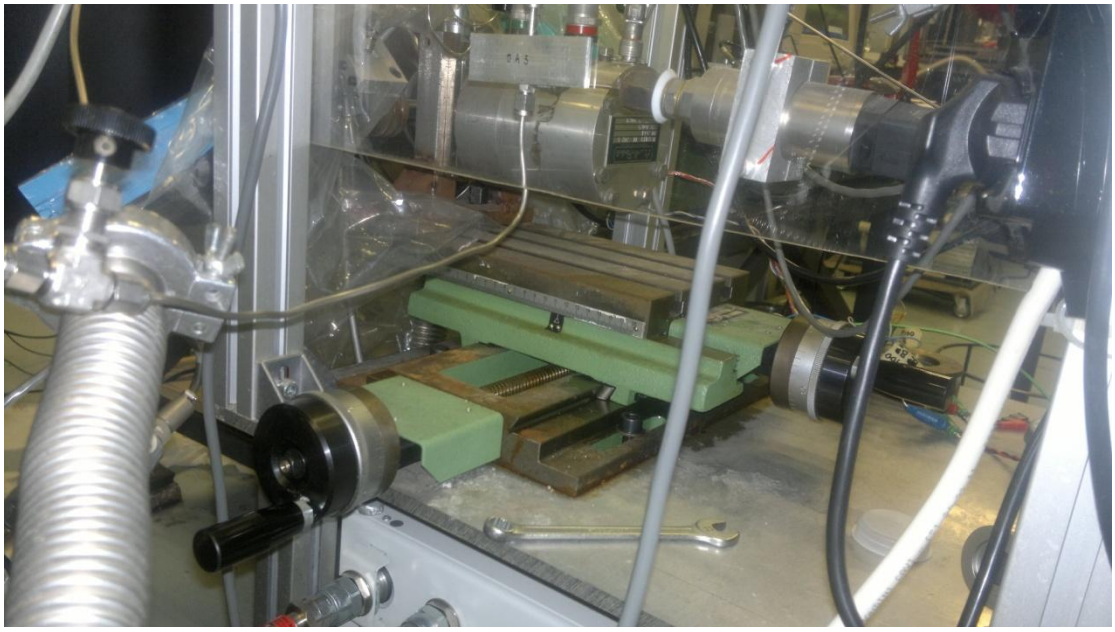

Figure 4.3. The overall system mounted on a movable rack, which can be easily aligned with the optical system during spectroscopic measurements.

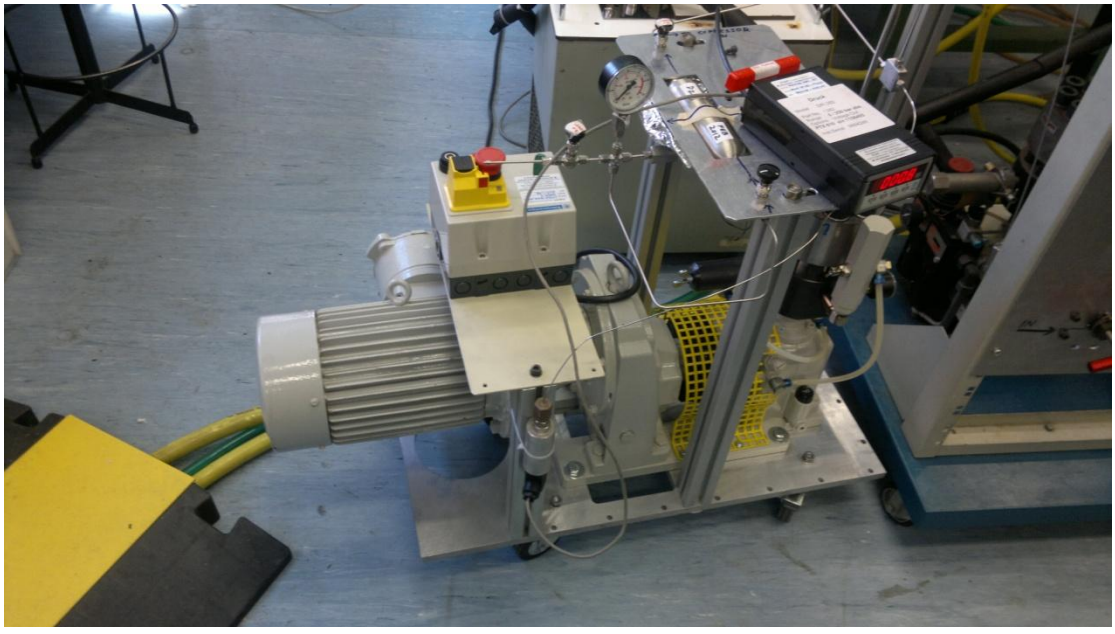

Figure 4.4. The Nova-Swiss membrane compressor that can raise the pressure of the gas up to 3500 bar.

Figure 4.5. Lakeshore DT 471 that is used to measure the temperature of the cell and another similar one is used to measure the temperature of the cold finger of the CCR.

Figure 4.6. The cryogenic device, capable of cooling the system down to 10 K.

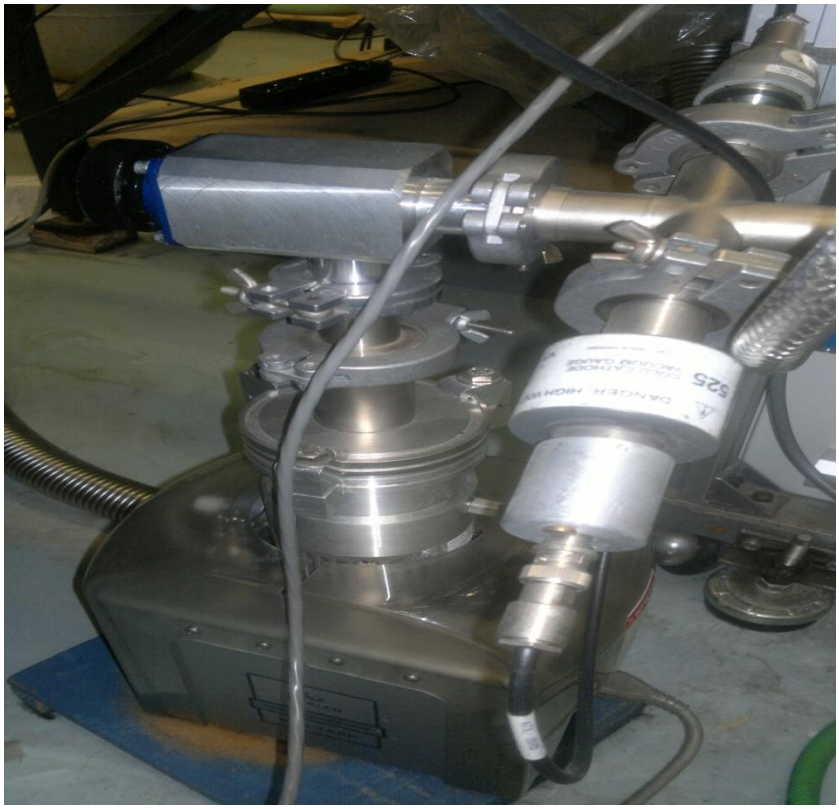

Figure 4.7. The evacuating pump connected with the cryogenic device.

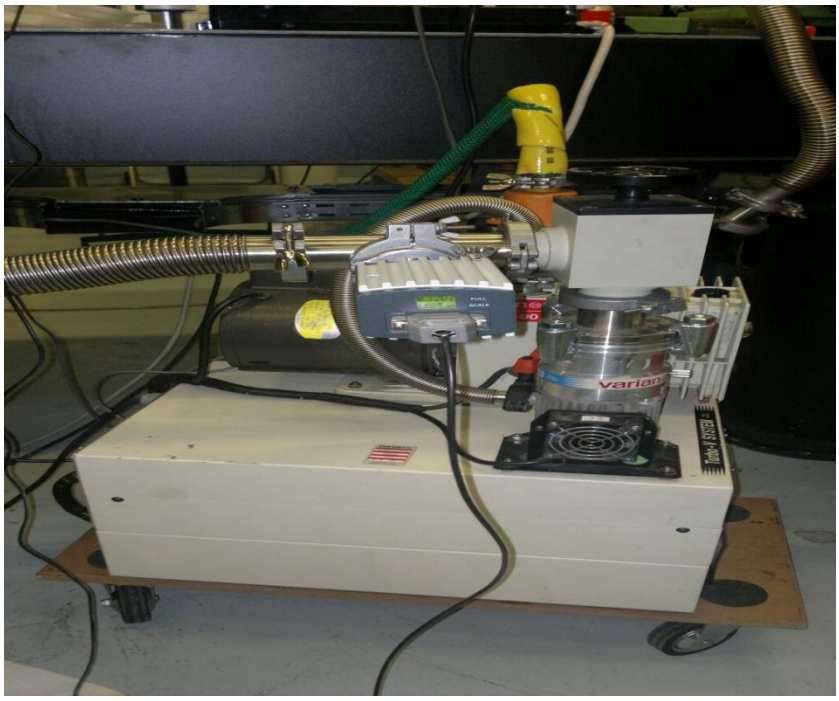

Figure 4.8. The turbomolecular pump that evacuate the steel chamber from atmospheric pressure to 8.32 x 10^{-7} mbar.

4.1.2 Optical Path Setup

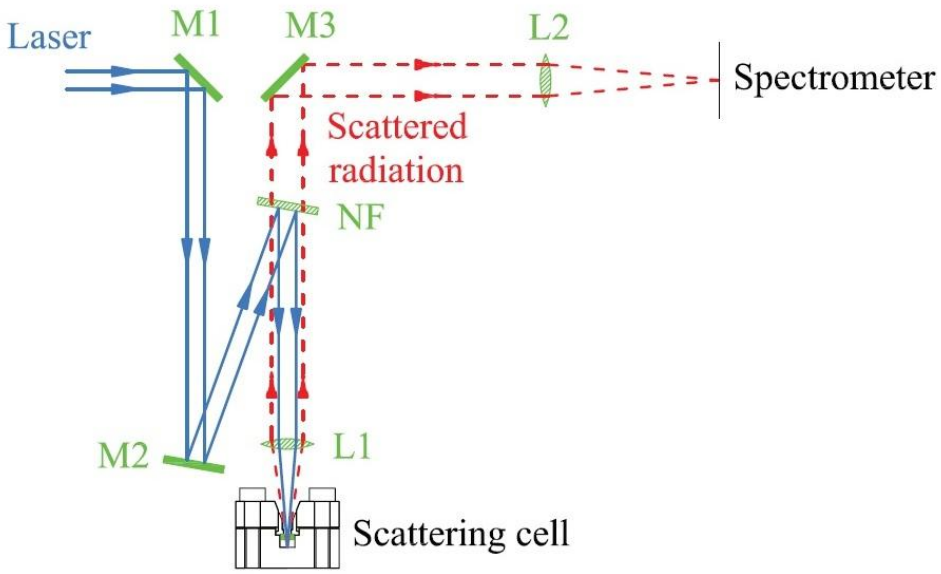

Figure 4.9. The optical path for back-scattering configuration**.** Incident laser beam path is blue and solid line, while the scattered beam path is red and dashed. M1, M2 and M3 are totally reflecting mirrors (aluminum-coated). L1 and L2 are collimating lenses. NF is a notch filter.

Figure 4.9 shows a schematic diagram of the optical setup used in this experiment. An argon laser beam, after being reflected by the two aluminum-coated mirror M1 and M2, reaches the notch filter that has an optimum working angle of 10^{o}. This notch filter reflects the incident laser beam but it allows the scattered beam to pass through it. Then, the laser beam is collimated into the sample using a L1 lens, that is, a 3 x microscope objective (70 mm focal length). The same lens collects the scattered beam and let it to pass through the notch filter to be reflected by M3 mirror. After that, a second collimating lens L2 is used to focus the radiation on the entrance slit of Spex triple-mate spectrometer. The lenses L1 and L2 have a magnification factor of five. The sample position (horizontal position) and focusing (vertical position) is aligned using a (infinite-adjusted) telescope to get high-resolution images. The same technique is used to adjust the focusing of the lens L2 on the

entrance slit of the spectrometer. A periscope, connected with a camera, is mounted inside the spectrometer to detect the laser spot resulted from scattering process of the sample. The Ar laser beam wavelength is 514.5 nm with a spot diameter of about 20 μm and a power on the sample surface of 45 mW. A diffraction grating is used to remove the plasma from the laser beam. All the optical tools are mounted on an optical bench. The Spex triple-mate spectrometer settings have been adjusted to get a high-resolution images (first slit width of 200 μm, second slit width of 50 μm, diffraction grating of 1800 grooves/mm). The CCD is calibrated at the vibrational and rotational bands of D_2 using a known spectra of a Neon lamp. Figure 4.10 show a wide picture of the assembly of the experiment components.

Figure 4.10. An assembly of the experiment components, (a) Ar laser, (b) the diffraction grating, (c) and (d) are aluminum coated mirror, (e) Lakeshore DT 471, (f) the steel vacuum chamber holding the cell mounted on a movable rack, (g) He Cryogenic system, (h) the position the of the cell under investigation, (i) CCD, (k) the turbomolecular pump, (l) the Spex triple-mate spectrometer.

Figure 4.11 shows the path of the scattered radiation inside the spectrometer. Figure 4.12 shows the Ar laser beam device. Figure 4.13 show the laser path in the back-scattering configuration. Figure 4.14 shows part of the pipeline system used in the experiment. Figure 4.15 shows Spex triple-mate spectrometer + CCD.

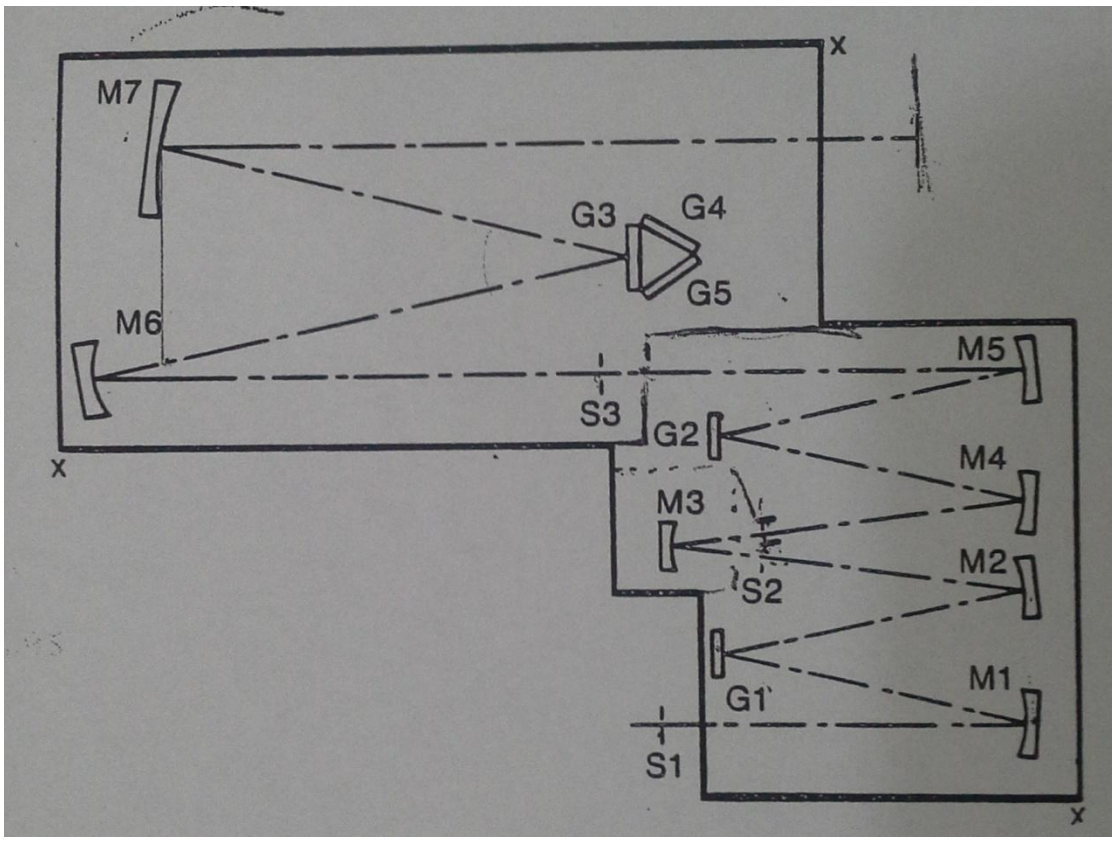

Figure 4.11. Shows the path of the scattered radiation inside Spex triple-mate spectrometer. The exit is connected with the CCD. All "G's" are gratings.

Figure 4.12. The Ar laser beam device.

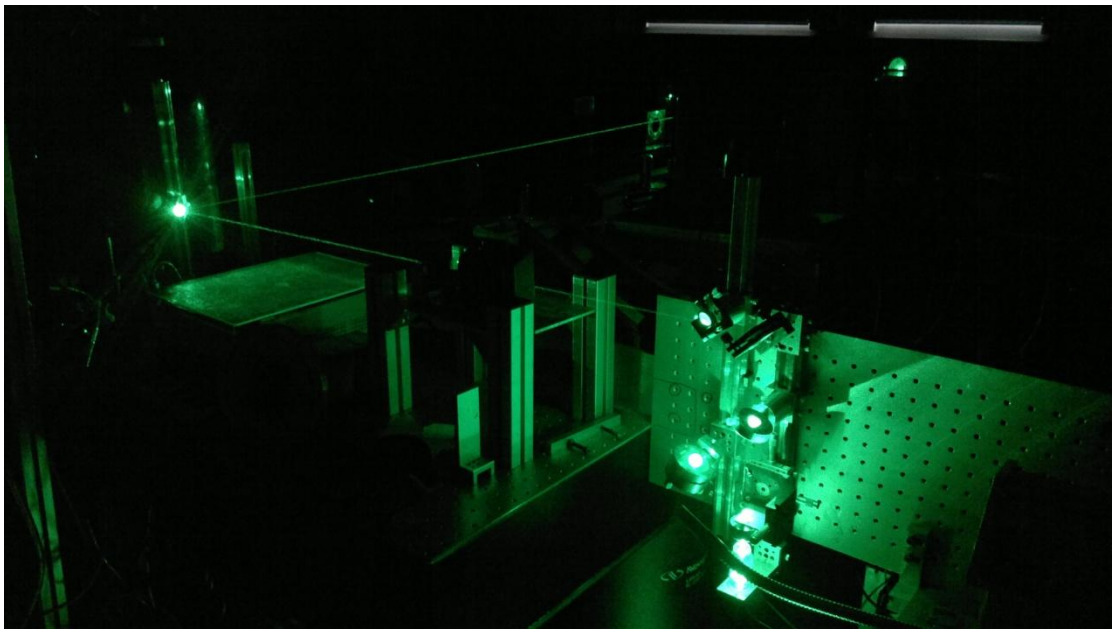

Figure 4.13. The path of the laser in the back-scattering configuration.

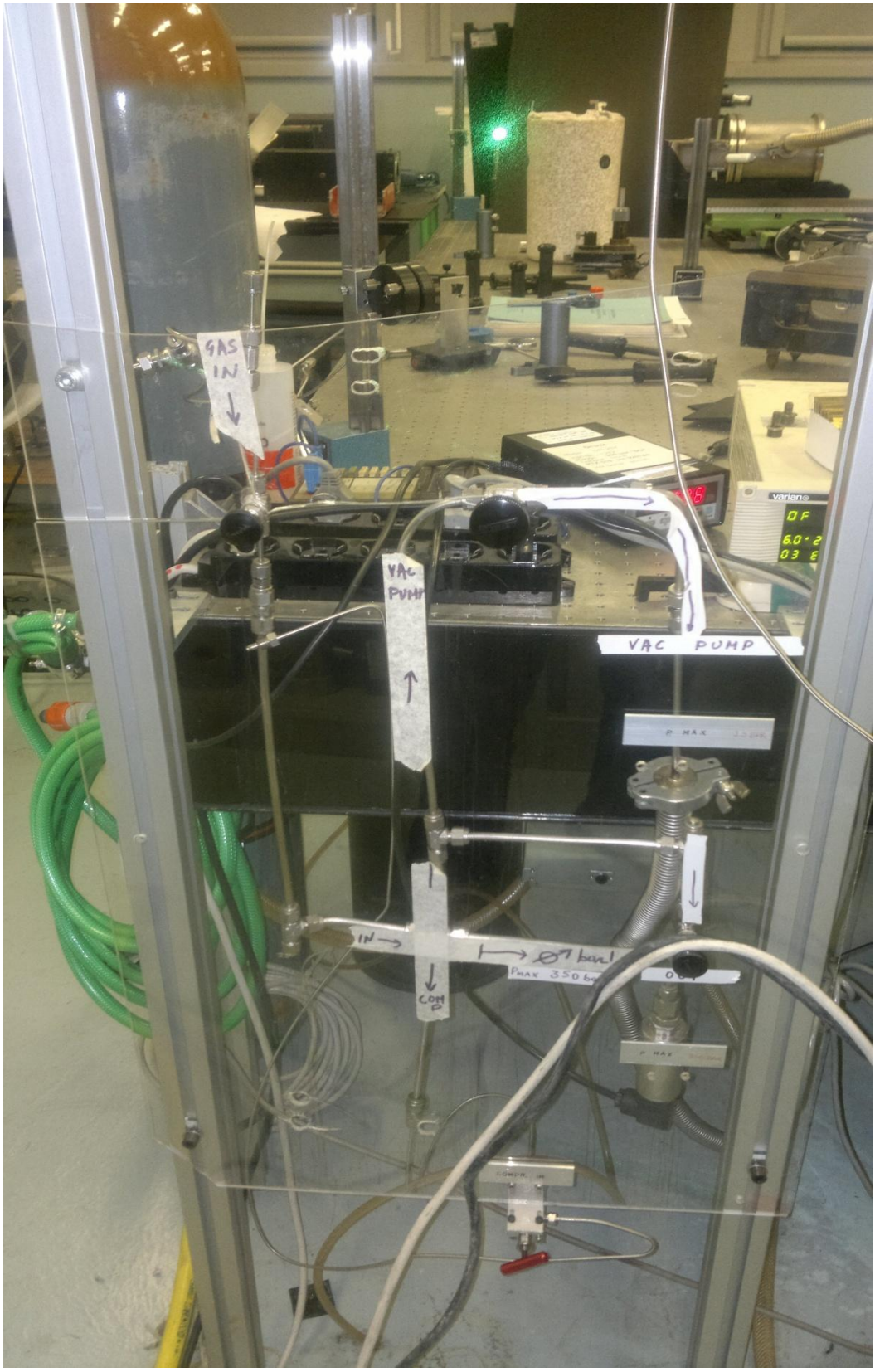

Figure 4.14. Part of the piplines used in the experiment.

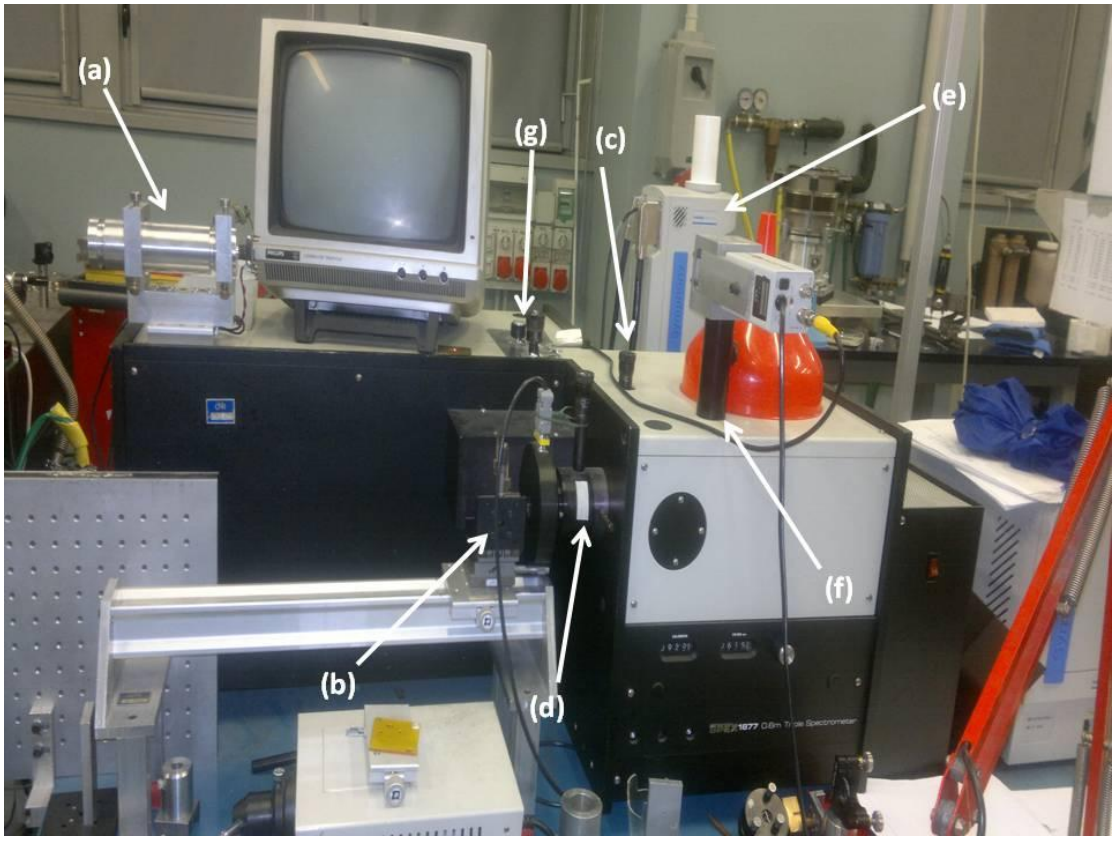

Figure 4.15. (a) is the infinite adjusted telescope used to adjust the position of the sample, (b) the second lens L2 that focus the image on the entrance slit of the spectrometer, (c) the second slit inside the spectrometer, (d) the first entrance slit, (e) Symphony CCD, (f) the periscope mounted inside the spectrometer and its image is shown on the monitor. (g) the diffraction grating resolution of the image (1800 gr/mm).

4.1.3 Procedure

To start investigating the deuterium hydrates, we put three distilled water drops in a small container inside the designed cell. Before mounting the flange into the cell body using screws to close the cell, we make sure that the diamond window is clean using ethanol solution to remove tiny particles on its surface. As we close the cell using screws, we must be very careful for the leveling of the flange because any small disturbance for the leveling on one side rather than the others may cause break of the diamond window. After closing the cell and inserting it in its position on the cryogenic arm, we put the copper shield that has a good thermal conductivity. After that, we fix the steel vacuum

chamber as an outer shield for the overall system making sure that its glass window is at the top of the position of the cell. The turbomolecular pump starts to evacuate the system outside the copper shield from the atmospheric pressure down to 8.32×10^{-7} mbar. To remove air particles from the cell, we pump a He gas inside the cell using the soldered capillary tube at pressure of around 40 bar and let it out again. We use He as a flushing gas for four times. Then, we adjust the position of the sample and the focusing using the (infinite-adjusted) telescope. We can move the sample using the movable rack by wheels. We let the D_2 gas to enter the cell with a pressure of 2124 bar. We leave the system for two days to let the gas to diffuse inside the water and to make the system stable. The Spex triple-mate spectrometer and the CCD are calibrated, at the vibrational (605-610 nm) frequency region to measure the vibrational Raman of D_2, or, at the rotational (518-523 nm) frequency region to measure the rotons of D_2, using a Ne lamp with known spectrum. If we are measuring at one region and want to move to another region, a new calibration is required. The calibration is done by taking the Raman spectrum of the neon lamp at the required region (acquisition of two and exposure time of two seconds in order to get sharp Raman spectrum without saturation of the CCD). If there is a shift between the Ne Raman lines and expected lines, we ask the computer to adjust the spectral lines at their correct positions. We let the Ar laser beam with low power (in order not to heat the sample) to fall on the sample after aligning the optical system and start taking the Raman lines.

To prepare the clathrate, we follow the P-T diagram (figure 1.11). We cool the all set using the cryogenic temperature control down to 266 K as a first step. As the temperature decreases, the pressure also decreases physically (pressure inside the cell become 1816 bar). Second step, we continue to cool the all set to 70 K. We start to evacuate the cell from the pressurized gas gradually (in steps of 50 bar) not suddenly until we have three bar. We leave very little amount of D_2 gas inside the cell to protect the sample from unexpected increase in the laser power. The clathrate is formed and we can study different Raman transitions.

4.2 Results and Data analysis

As we mentioned before, the problem of Raman spectrum explanation of clathrate hydrate is the assignment of occupancies per cages. In simple hydrate, there are small cages and large cages. The small cages can trap only one deuterum molecule. On the other hand, the large cages can host, two, three or four molecules according to Strobel , [33] or, one, two or three molecules according to Giannasi. [36] The small cages frequencies are lower than the large cages frequencies. As the cage accommodates more molecules, as the Raman peaks of these cages appear at higher frequencies.

The intensities of Raman spectral lines depend on the population of molecules at the different energy states. Therefore, to investigate the population of D_2 molecules at these states, Raman spectrum at the rotational region of D_2 should be collected. Figure 4.16 shows the rotational spectrum of D_2 hydrate at 70 K and 20 K. From this figure, it is clear that the first three $S_o(0), S_o(1)$ and $S_o(2)$ transitions are existing at 70 K, while, at 20 K, the $S_o(2)$ transition disappears. This happens because the energy state that allows $S_o(2)$ transition becomes unpopulated at very low temperatures (like 20 K). As a result, D_2 molecule will have only two rotational transitions at this specific temperature. From the last conclusion, we expect that each deuterium occupancy will contribute with two vibrational lines (*ortho* and *para*) with a separation of approximately 2 cm^{-1}.

In our laboratory, we have performed high resolution Raman measurements for the simple D_2 hydrate. Each spectrum is collected through the CCD with a specific acquisition and exposure time. The acquisition and exposure time depend on the signal to noise ratio. Then, the collected spectrums are fitted using Origin 8.6 Peak fitting module. The fitting process is a theoretical process that shows the way that each deuterium molecule per cage will contribute to give the full experimental Raman spectrum. To do fitting for a

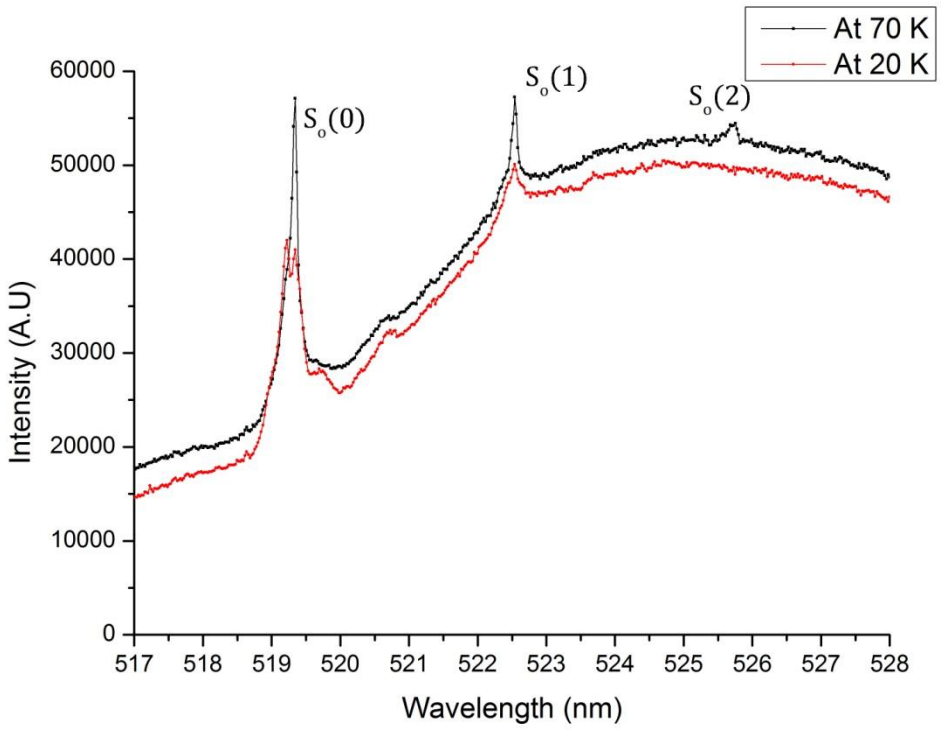

Figure 4.16. The rotational spectral lines of D_2 simple clathrate at 20 and 70 K.

D_2 Raman spectra, we should apply two constraints. First, the distance between the center of *ortho* curve and *para* curve for the same molecule is 2 cm^{-1}. Second, the all Gaussians must have the same full width at half maximum (FWHM).

Figure 4.17 shows the result of peak fitting for Raman spectrum of D_2 simple clathrate collected at 20 K. We have used eight Gaussians to interpret the Raman peaks in the large cages instead of six stated by Strobel or Giannasi. We suggest that D_2 will occupy the large cages with one, two, three and four molecules. This model can be considered as a combination of both Strobel and Giannasi models. Actually, we cannot apply either Strobel model or Giannasi model. If we apply Strobel or Giannasi assignment, we will find an extra peak (its center ~ 2990 cm^{-1}) without any assignment to a specific occupancy.

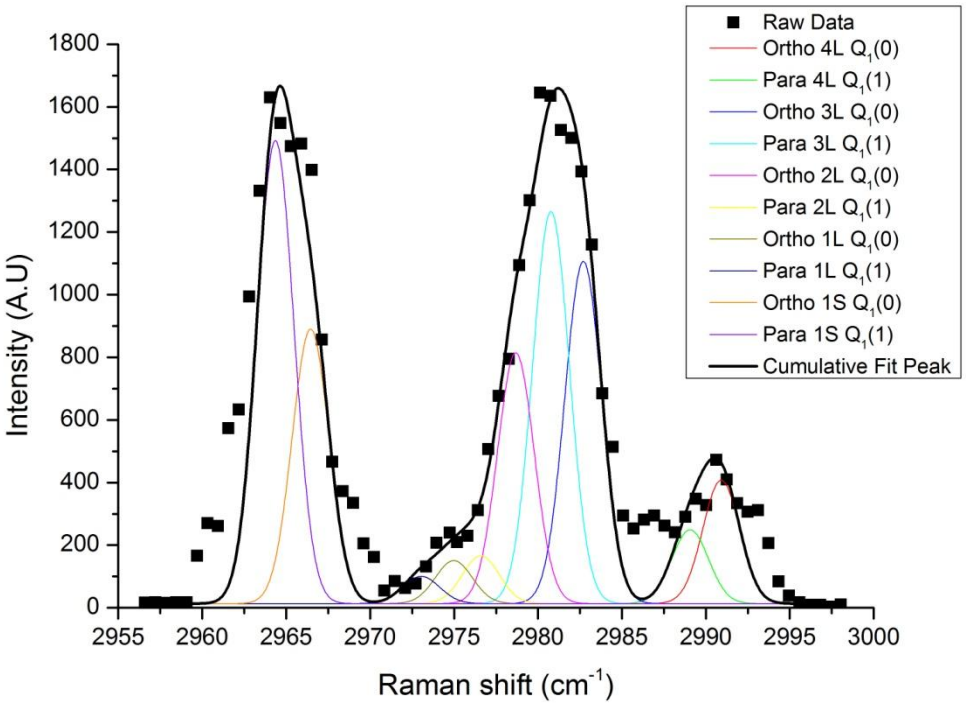

Figure 4.17. Fitted Raman spectra of simple D_2 hydrate formed at 1816 bar and 266 K, and collected at 20 K. Constraints were forced on the fit such that each Gaussian pair should have the 2 cm^{-1} frequency separation and all Gaussians should have the same FWHM. The introduced assignment of the large cages is 1L, 2L, 3L and 4L. As shown in the figure, each occupancy has both *ortho* and *para* Gaussians.

So that, we have introduced the 1L occupancy (one D_2 molecule occupies the large cage). The new assignment has been elucidated by heating/quenching cycles. Heat/quench cycle means heating the sample to a specific temperature (90 K as an example) and cooling the sample to the original temperature. Heat/quench cycles forces some deuterium molecules to get out from their cages and occupy neighboring cages with lower occupancies. For example, if we have a D_2 molecule in a 3L cage, upon heating, it may transfer to 2L or get out the clathrate. Heating the sample can provide more sharp images with high resolution. By applying heat/quench cycle for the last fitted spectrum, we get the new spectrum shown in figure 4.18.

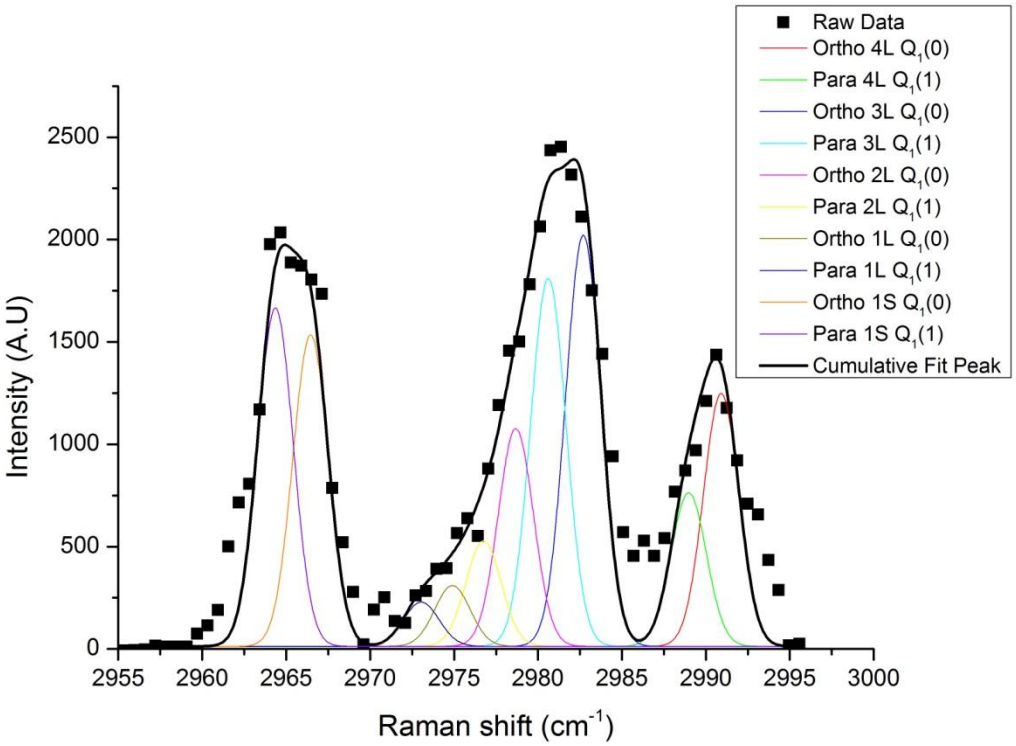

Figure 4.18. New fitted Raman spectrum of D_2 hydrate, formed at 266 K and 1816 bar, measured at 20 K. After applying heat (90 K)/quench cycle (20K), we can notice the strong appearance of the shoulder at around 2980 cm^{-1}. In addition, we can notice the supposed increase in the intesity of 2L.

Upon heating the sample, some molecules of 3L cages get out and move to 2L cages making the intensity of the 2L larger, and increasing the intensity of shoulder strongly (at 2980 cm^{-1}) as shown in figure 4.18. In addition, heating of the sample makes the molecules more energetic and some *ortho-para* conversion occurs. *Ortho-para* conversion can be happen as a function of time too. Figure 4.19 shows the Raman spectrum of D_2 hydrate after three days. From the graph, we can notice the rise of a peak at 2972.5 cm^{-1}. The rise of this peak has been explained as a result of some *ortho-para* conversion. This conversion has been done within three days.

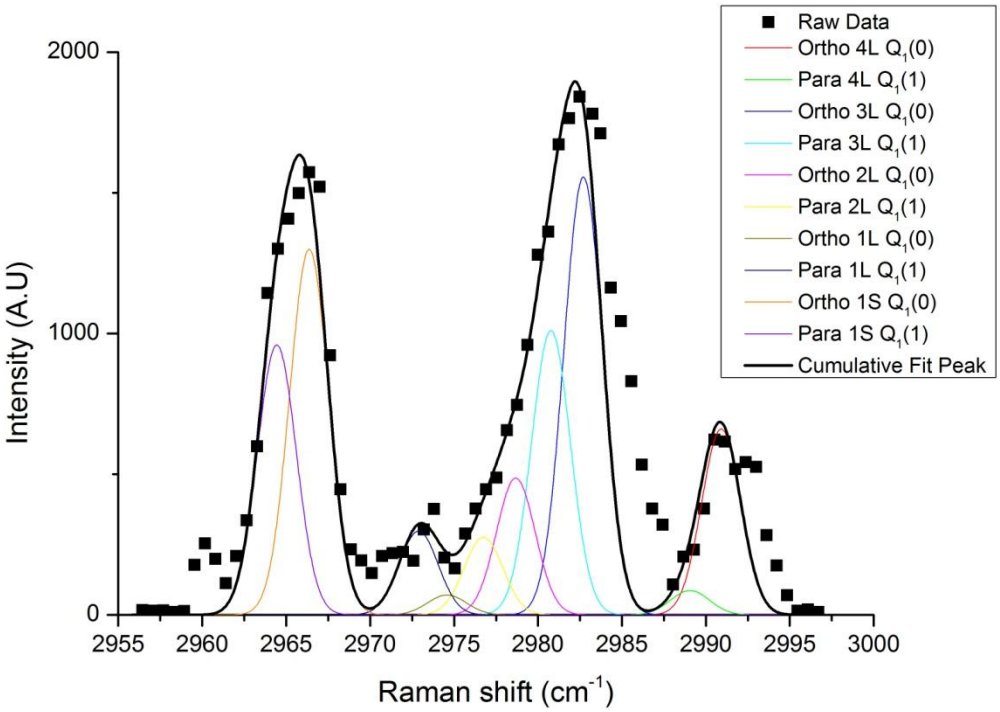

Figure 4.19. *Ortho-Para* conversion occurs within three days after the formation of D_2 hydrate formed at 1816 bar and 266 K. The appearance of the new peak at ~ 2972.5 cm^{-1} has been introduced as a result of this conversion.

After applying another thermal treatment (heating up to 100 K and cooling to 20 K again), it is clear that the 2L and 1L peaks have higher intensities than before. The shoulder at ~ 2976 cm^{-1} is the cumulative Raman spectra of both 1L and 2L. Therefore, we can notice the decrease in the 3L intensity. The 4L and 1L remain approximately unchanged because they are away of the cluttered region that host 3L and 2L (there is strong interaction of molecules and cages in this region) but, generally, their intensities decrease. Figure 4.20 shows the effect of applying second heat/quench cycle.

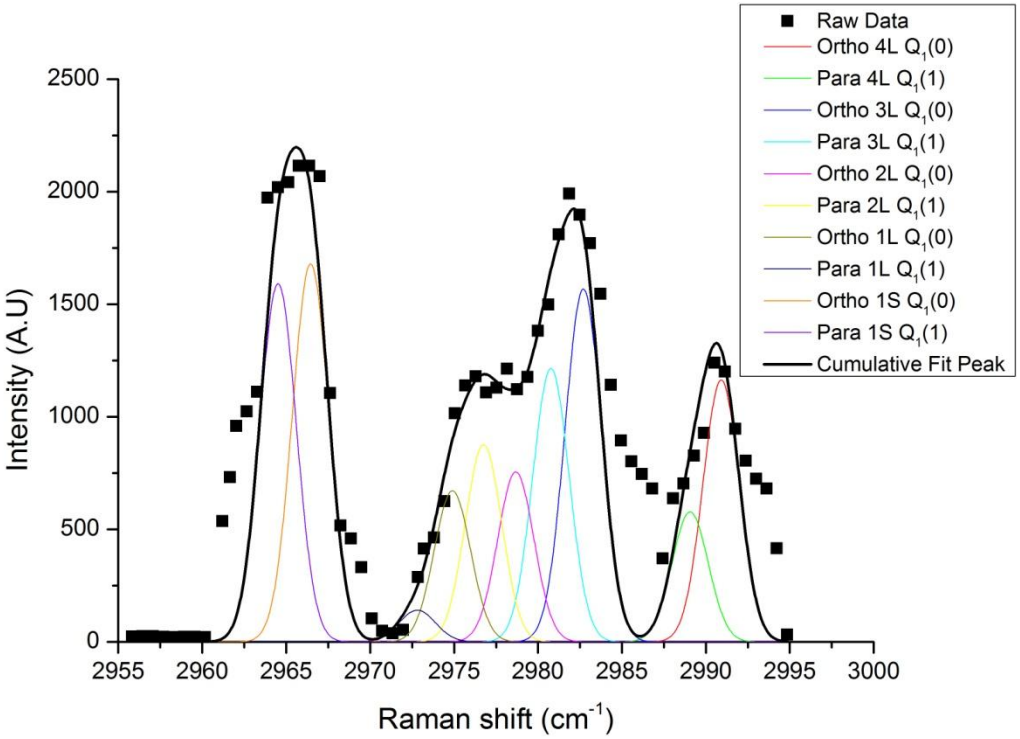

Figure 4.20. New fitted Raman spectrum of D_2 hydrate, formed at 266 K and 1816 bar, measured at 20 K. After applying second heat (100 K)/quench cycle (20K), we can notice the strong appearance of the shoulder at around ~ 2976 cm^{-1}. In addition, we can notice the supposed increase in the intesity of 2L and 1L.

We can get more resolution and further confirmation of the supposed assignment by applying third heat/quench cycle. We cannot heat the sample to 100 K in order not to destroy the clathrate because the clathrate will be destroyed if the 3L cages have been dissociated, and, with heating the sample up to 100 K, will help 3L molecules to get out more, and hence, destroying the clathrate. Therefore, we will heat the sample up to 45 K only. Before doing the heat treatment, we let some of free D_2 gas trapped inside the cell to get out in order not to contribute in the resulted Raman spectrum. Figure 4.21 show the Raman spectra of simple D_2 hydrate after the third heat treatment. As shown in the graph 4.21 the intensity of the 3L has been decreased considerably. It

becomes very close to the 2L intensities and slightly higher than the 1L intensities. This confirms our assignment for the large occupancies of 1L, 2L, 3L and 4L.

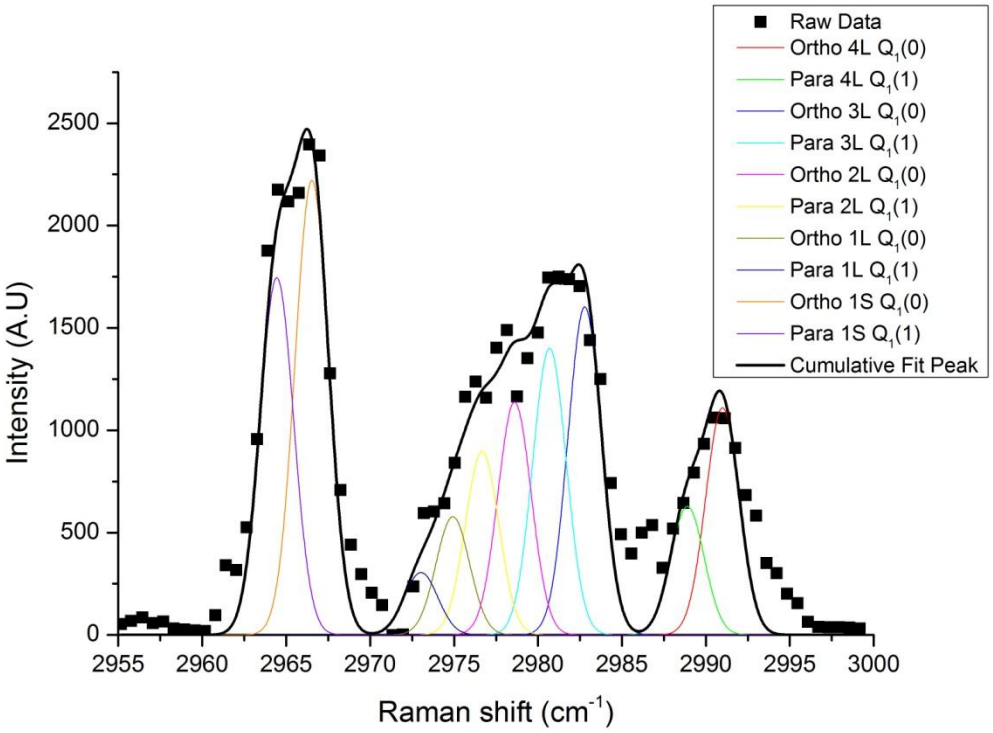

Figure 4.21. Fitted Raman spectrum of D_2 hydrate, formed at 266 K and 1816 bar, measured at 20 K. After applying third heat (45 K)/quench cycle (20K), we can notice the growth of 1L and 2L intensities. In addition, we can notice the decrease in the intesity of 3L.

Figure 4.22 shows overall combination of D_2 Raman spectrums under investigation in this research with respect occupancies per cages.

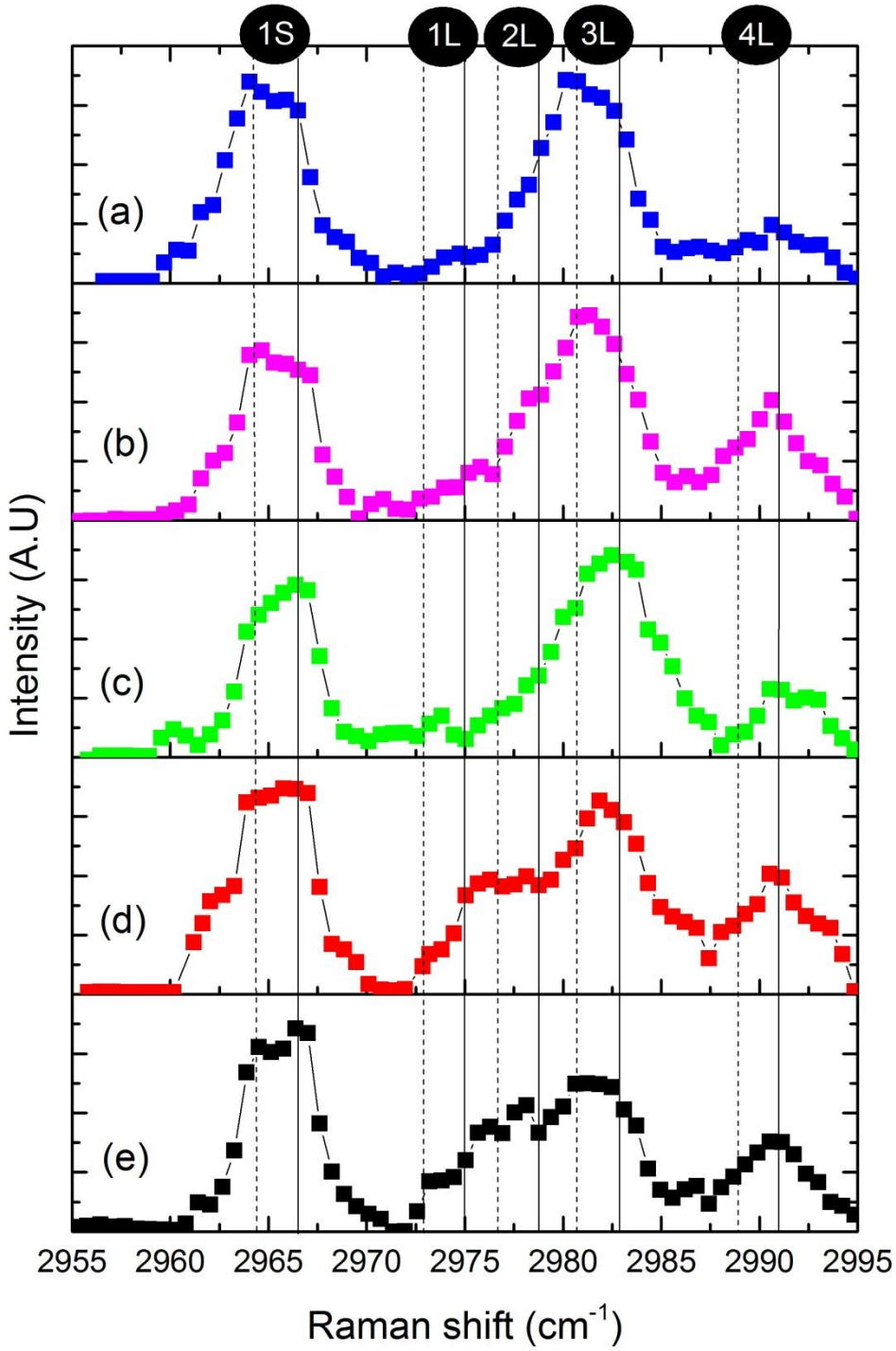

Figure 4.22. An overall view of Raman spectrums resulted by simple D_2 hydrate sample synthesised at 1816 bar and 266 K, measured at 20 K. (a) represents the simple hydrate *in-situ* prepared. (b) the sample after one heat (90 K)/quench (20 K) cycle. (c) is the same conditions of (b) but after three days. (d) the sample after a second heat (100 K)/quench (20K) cycle. (e) the Raman spectra after the third heat (45 K)/quench (20 K) cycle. The position of each Gaussian is clarified.

4.3 Conclusion

$D_2 + H_2O$ simple hydrate has never been investigated before; therefore, a sample, prepared at 1816 bar and 266 K, has been synthesized *in-situ.* Raman measurements have been performed to the sample before and after many heating/quenching cycles. The measurements are taken at 20 K. Peak fitting tool has been utilized to help predicting the individual contribution of each occupancy per cage. Applying constraints on the Gaussian curves in order to help predicting correctly. The Gaussian curves consist of a pair of peaks represent *ortho* and *para* transitions of the molecule. The constraints are fixing the separation between *ortho* and *para* to be 2 cm^{-1}, and assuming that all Gaussians must have the same FWHM.

A new assignment for the large cages occupancies has been introduced. Without the new assignment, we cannot interpret the Raman spectra correctly. There will be additional unassigned peak according to old models. The new assignment suggests that large cages can host one, two, three and four molecules. This assignment has been confirmed using heat/quench cycle. By applying any heat/quench cycle, the molecules in large cages tend to get out of the cage and move to a neighboring cage with lower occupancy number. By using this concept, we have explained the formation of 1L peaks. In addition, the clathrate will be destroyed in case of complete dissociation of 3L.

In addition, *ortho-para* conversion has been observed. It is shown that it depends on the temperature change in addition to being a function of time.

Chapter 5 APPLICATIONS AND RECOMMENDATIONS FOR FUTURE WORK

There are many applications can be initiated based on clathrate compounds. In this chapter, some possible applications will be introduced. In addition, recommendations for future research work will be presented to create new horizons regarding the physics and chemistry of the clathrates and to overcome some technical problems regarding the usage of clathrate compounds in industry or in our life.

5.1 Commercial and Industrial Applications

Although the science of clathrates is an old science, we could not make use of it until now. We still in need to investigate clathrates chemical and physical aspects because we do not know exactly how they are formed or dissociated. By the available knowledge regarding the clathrates, we expect that clathrates can be used to store and transport gases like H_2, CH_4, and C2H6… Etc. In addition, the huge amount of clathrates in nature can be used as a future clean fuel.

5.1.1 Storage and Transport

Clathrates can be used to trap molecules of different sizes. Recently, it is found that they can store hydrogen and form stable compounds. Therefore, scientists suggest the clathrates as a potential storage material.

5.1.2 Energy Reservoir

Methane hydrate is an abundant with a reservoir of around 6.4 trillion tons presented on ocean floor. [17] This huge amount is twice the amount of carbon found in all known fossil fuel sources. This amount still negligible although it can cover the world needs for decades.

5.1.3 Solving Environmental Problems

Clathrates can be used to solve some environmental problems. The excess presence of CO_2 gas represents a very big problem because it plays an important role in the green house effect. We can reduce the CO_2 percentage by forming carbon dioxide hydrates.

5.1.4 Method of Separation

The clathrate hydrate can be used to separate a specific material from a mixture of materials. If we have a mixture of gases for example, we can trap a definite gas from this mixture inside the clathrate cages. In addition, the formation process of the clathrate depends on the applied pressure, temperature and the size of the guest molecule. Therefore, by applying the required conditions, the clathrate will be able to choose a particular guest molecule and reject the others.

5.2 Recommendations for Future Work

To open a new area of clathrate research, new concepts must be introduced in addition to develop the known knowledge and theories. The development must be in two ways, experimentally and theoretically.

Multiple occupancy per cage has opened new horizons for clathrate research. H_2, Ne, and He can occupy the large cages with multiple molecules. This needs further investigation to develop a new clathrate that can provide high energy density. In addition, the enclathration of two or more guest molecules inside one large cage is a new challenging research interest. It may provide solutions for some technical problems and innovate new materials that can replace normal fossil fuel.

The influence of a second guest molecule in binary clathrates on small cavity hydrogen filling needs more investigation. THF + H_2 and cyclohexanone + H_2 propose perfect cavity size for optimized H_2-H_2O interaction. This idea may be experimentally experienced by forming several binary clathrate hydrates with hydrogen and a second guest of varying size. This second guest will occupy the large cage and affects the lattice parameters allowing us to study this effect.

Molecular simulations are needed to give insight view regarding the ability of molecule to occupy a clathrate cage. In addition, they can provide some explanation regarding the unexpected experimental data.

REFERENCES

[1] Sloan, E.D., and Koh, C.A. 2008. *Clathrate Hydrates of Natural Gases 3rd Edition*. Boca Raton, FL: CRC - Taylor Francis.

[2] Strobel, T. A. ; Hester, K. C.; Koh, C. A.; Sum, A. K. and Sloan, J. E. D.; "Properties of the Clathrates of Hydrogen and Developments in their Applicability," *Chemical Physics Letters,* vol. 478, no. 4-6, pp. 97-109, 27 August 2009.

[3] W. L. Mao ; C. A. Koh, and E. Dendy Sloan. 2007. Clathrate Hydrates Under Pressure, Phys. Today 60, 42, DOI:10.1063/1.2800096.

[4] Davidson, D.W. 1979. Clathrate Hydrates. *Pages 115-234 of:* Franks, F. (ed), *Water: A Comprehensive Treatise*, vol. 3. New York: Plenum Press.

[5] V. Stackelberg, M., Naturwiss. 36, 359 (1949).

[6] McCarty, R.D. 1975. *Hydrogen Technological Survey - Thermophysical Properties*. Tech. rept. Scientific and Technical Information Office.

[7] Holder, G.D., Stevenson, L.J., Joyce, J.J., John, V.T., and Kamath, V.A. 1983. Formation of Clathrate Hydrates in Hydrogen-Rich Gases. *Ind. Eng. Chem. Des.Dev.*, 22, 170-171.

[8] Strobel, T. A.; Sloan, E. D. and Koh, C. A.; "Raman spectroscopic studies of hydrogen clathrate hydrates," *The Journal of Chemical Physics,* vol. 130, p. 014506, January 2009.

[9] Strobel, T. A.; Taylor, C. J.; Hester, K. C.; Dec, S. F.; Koh, C. A.; Miller, K. T. and Sloan, E. D.; "Molecular Hydrogen Storage in Binary THF−H2 Clathrate Hydrates," *The Journal of Physical Chemistry B,* vol. 110, no. 34, p. 17121, August 2006.

[10] Strobel, T. A.; Sloan, E. D. and Koh, C. A.; "Water Cavities of sH Clathrate Hydrate Stabilized by Molecular Hydrogen," *Journal of Physical Chemistry B,* vol. 112, no. 885, p. 1885–1887, 2008.

[11] Dyadin, Y.A., Larionov, E.G., Manakov, A.Y., Zhurko, F.V., Aladko, E.Y., Mikina, T.V., and Vladislav, Y.K. 1999b. Clathrate hydrates of hydrogen and neon. *Mendeleev Commun.*, 5, 209-210.

[12] Dyadin, Y.A., Larionov, E.G., Aladko, E.Y., Manakov, A.Y., Zhurko, F.V., Mikina, T.V., Komarov, V.Y., and Grachev, E.V. 1999a. Clathrate Formation in Water-Noble Gas (Hydrogen) Systems at High Pressure. *J. Struct. Chem.*, 40, 790-791.

[13] Mao, W.L., Mao, H.K., Goncharov, A.F., Struzhkin, V.V., Guo, Q.Z., Hu, J.Z., Shu, J.F., Hemley, R.J., Somayazulu, M., and Zhao, Y.S. 2002. Hydrogen clusters in clathrate hydrate. *Science,* 297(5590), 2247. Article SCIENCE.

[14] Subramanian, S., and Sloan, E.D. 2002. Trends in vibrational frequencies of guests trapped in clathrate hydrate cages. *J. Phys. Chem. B*, 106(17), 4348-4355.

[15] Lokshin, K.A., Zhao, Y., He, D., Mao, W.L., Mao, H., Hemley, R.J., Lobanov, M.V., and Greenblatt, M. 2004. Structure and dynamics of hydrogen molecules in the novel clathrate hydrate by high pressure neutron diffraction. *Phys. Rev. Lett.*, 93(12), 125503-1.

[16] Ishmaev, S.N., Sadikov, I.P., Chernyshov, B.A., Vindryaevskii, V.A., Sukhoparov, A.S., and Kobelev, G.V. 1983. Neutron Structural Investigations of Solid Parahydrogen at Pressures up to 24 kbar. *Sov. Phys. JETP*, 84, 228.

[17] Buffett, B.; Archer, D. (2004). "Global inventory of methane clathrate: sensitivity to changes in the deep ocean". *Earth Planet. Sci. Lett.*: 185–199.

[18] Satyapal, S., Read, C., Ordaz, G., and Thomas, G. 2006. Hydrogen Storage. *In: Annual DOE Hydrogen Program Merit Review*.

[19] Lokshin, K.A., and Zhao, Y. 2006. Fast Synthesis and Phase Diagram of Hydrogen Clathrate Hydrate. *Appl. Phys. Lett.*, 88, 131909.

[20] Vos, W.L., Finger, L.W., Hemley, R.J., and Mao, H-K. 1993. Novel H2 - H_2O Clathrates at High Pressures. *Phys. Rev. Lett.*, 71, 3150-3153.

[21] Natarajan V, Bishnoi PR, Kalogerakis N. Induction phenomena in gas hydrate nucleation. Chem Eng Sci 1994;49:2075e87.

[22] Ribeiro CP, Lage PLC. Modelling of hydrate formation kinetics: state-of-the-art and future directions. Chem Eng Sci 2008;63:2007e34.

[23] Groen CB. CO2 hydrate formation in coil heat exchangers. Delft: Delft University of Technology; 2012.

[24] A. T. Trueba, I. R. Radović, J. F. Zevenbergen, C. J. Peters, M. C. Kroon, Kinetic measurements and in situ Raman spectroscopy study of the formation of TBAF semi-hydrates with hydrogen and carbon dioxide, International Journal of Hydrogen Energy, Volume 38, Issue 18, 18 June 2013, Pages 7326-7334, ISSN 0360-3199.

[25] Yokoyama H, Kannami M, Kanno H. Chem Phys Lett 2008; 463:99.

[26] Duarte, A. R. C.; Shariati, A.; Rovetto, L. J. and Peters, C. J.; "Water Cavities of sH Clathrate Hydrate Stabilized by Molecular Hydrogen: Phase Equilibrium Measurements," *J. Phys Chem B*, 2008, 7, 1888.

[27] H. Hermann, and Hans Christoph Wolf. Molecular Physics and Elements of Quantum Chemistry. 1st ed. Berlin Heidelberg New York: Springer-Verlag, ISBN 978-3-662-03075-2, 1995.

[28] Zaghloul, M. A., Study of the Raman Spectrum of Simple Clathrate Hydrates of Hydrogen, M.Sc thesis, Faculty of Engineering, Cairo University, 2011.

[29] Long, D., " The Raman Effect: A Unified Treatment of the Theory of Raman Scattering by Molecules," 2002.

[30] J. Aleksander, "Efficiency of Anti-Stokes Fluorescence in Dyes," Nature, volume 131, pp. 839-840, 1933.

[31] Podolsky, B. 1928. *Phys. Rev.* 32: 812, doi:10.1103/PhysRev.32.812.

[32] Herzberg, G. 1939. *Molecular Spectra and Molecular Structure I. Diatomic Molecules*. New York: Prentice-Hall.

[33] Strobel, T. A., On Some Clathrates of Hydrogen, PhD thesis, Colorado School of Mines, Colorado University, 2008.

[34] Van Kranendonk, J. 1983. *Solid Hydrogen*. New York: Plenum.

[35] Giannasi, A.; Celli, M., Zoppi, M.; Moraldi M. and Ulivi, L.; "Experimental and Theoretical Analysis of the Rotational Raman Spectrum of Hydrogen Molecules in Clathrate Hydrates," *Journal of Chemical Physics,* vol. 135, no. 5, p. 054506, August 2011.

[36] Giannasi, A.; Celli, M. and Ulivi, L.; "Low Temperature Raman Spectra of Hydrogen in Simple and Binary Clathrate Hydrates," J. Chem. Phys. 2008, 8, 084705.

[37] T. A. Strobel, C. A. Koh and E. D. Sloan, "Hydrogen Storage Properties of Clathrate Hydrate Materials," *Fluid Phase Equilibria*, vol. 261, pp. 382-389, 2007.

[38] Milva Celli, Marco Zoppi, Mohamed A. S. Zaghloul, and Lorenzo Ulivi, High pressure optical cell for synthesis and in situ Raman spectroscopy of hydrogen clathrate hydrates, Rev. Sci. Instrum. 83, 113101 (2012), DOI:10.1063/1.4764531.